ABSTRACT

Title of Thesis:	NUMERICAL CHARACTERIZATION AND MODELING OF ADIABATIC SLOT FILM COOLING
	Andrew Voegele, M.S. 2011
Directed By:	Associate Professor André W. Marshall Department of Fire Protection Engineering, Adjunct Faculty of Aerospace Engineering Department

Film cooling is a technique used to protect critical surfaces in combustors, thrust chambers, turbines and nozzles from hot, chemically reacting gases. Accurately predicting the film's performance is especially challenging in the vicinity of the wall and the film injection plane due to the complex interactions of two highly turbulent, shearing, boundary layer flows. Properly characterizing the streams at the inlet of a numerical simulation and the choice of turbulence model are crucial to accurately predicting the decay of the film. To address these issues, this study employs a RANS solver that is used to model a film cooled wall. Menter's baseline model, and shear-stress transport model and the Spalart-Allmaras model are employed to determine the effect on film cooling predictions. Several methods for prescribing the inlet planes are explored. These numerical studies are compared with experimental data obtained in a UMD film cooling wind tunnel.

NUMERICAL CHARACTERIZATION AND MODELING OF ADIABATIC SLOT
FILM COOLING

by

Andrew Voegele

Thesis submitted to the Faculty of the Graduate School of the
University of Maryland, College Park in partial fulfillment
of the requirements for the degree of
Masters of Science
2011

Advisory Committee:

    Associate Professor André W. Marshall, Chair
    Associate Professor Arnaud Trouvé
    Associate Professor Christopher Cadou
    Associate Professor Kenneth Yu

Acknowledgements

TABLE OF CONTENTS

List of Tables

List of Figures

Nomenclature

Roman
b　　　height of mixing layer
BR　　 blowing ratio
c_p　　specific heat
CV　　 control volume
dV　　 differential elemental volume
dS　　 differential elemental area
e　　　internal energy
h　　　enthalpy
I　　　identity tensor
k　　　turbulent kinetic energy, thermal conductivity
L　　　length
n　　　normal vector
P,p　　pressure
Pr　　 Prandtl number
q　　　heat flux
Re　　 Reynolds number
s　　　slot height
t　　　time
T　　　temperature
U,u　　velocity vector, streamwise velocity component
V　　　diffusion velocity
v　　　vertical velocity component
VR　　 velocity ratio
x　　　streamwise coordinate
y　　　wall normal coordinate

Greek
ε　　　eddy dissipation
δ　　　delta vector
δ　　　characteristic length
η　　　effectiveness
μ　　　viscosity
ρ　　　density
τ　　　shear stress
ω　　　specific dissipation

Subscripts
ad　　 adiabatic wall
aw　　 adiabatic wall
c　　　coolant region
flow　 flow/fluid region
s　　　coolant region/slot region
t　　　turbulent

τ	frictional units
∞	mainstream
+	wall units

Superscripts

`	fluctuating component
-	averaged or filtered
``	flux
.	time flux

Chapter 1: Introduction

A major design challenge in modern combustion-based propulsion systems is the effective cooling of critical components from high thermal loads. In general as the operating temperature and pressure increase, the cycle efficiency of these engines is boosted. This improved efficiency is constrained by material limits, requiring reliable cooling for efficient, durable operation. One technique that is used to extend these limits is film cooling, which involves injecting a coolant gas along a surface to create an insulating layer that protects the walls from the hot combustion gases. Rocket engines feature ablative, regenerative, film and radiation cooling. A sample film cooling scheme for rocket engines is shown in Figure 1, where the nozzle thrust assembly and nozzle wall are cooled. In gas turbine engines, bleed air is injected through small holes and slots to convectively cool the combustor liner and turbine blades, along with radiative cooling to the outer casing. A schematic of a combustor liner design is shown in Figure 2. For modern gas turbine engines, Lefebvre[2] estimates that approximately one-third of the total combustor airflow is used to cool the combustor liner. The different cooling processes cause a total pressure drop, a reduction of air used for tailoring exit

Figure 1. Film Cooling schematic of a rocket
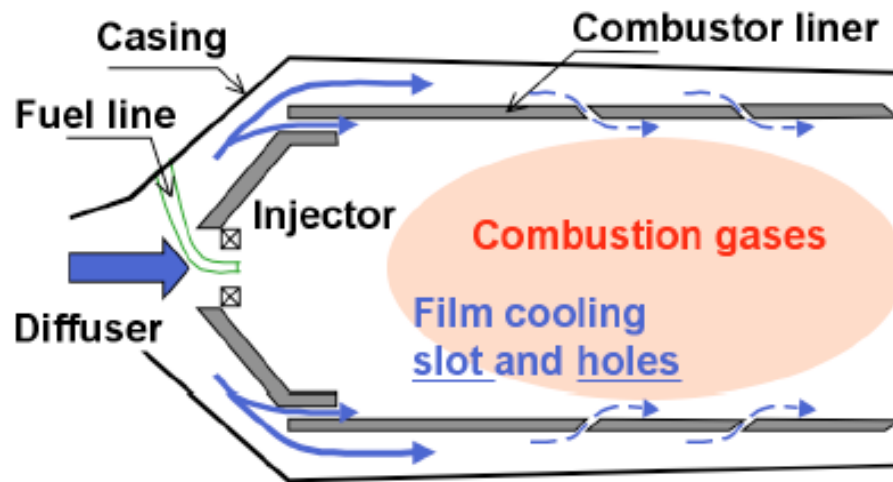
Figure 2. Film cooling schematic of a gas turbine engine combustor (adapted from Raffan[3]).

combustor temperatures through dilution, and a decrease in the combustion efficiency due to quenching, which leads to an increase in the emissions of pollutants. Decreasing the amount of cooling air, while maintaining adequate protection of key surfaces, has the potential to make propulsion systems more efficient and cost effective.

Film cooling is an important cooling mechanism in the J-2X liquid rocket engine where exhaust from the fuel turbopumps is injected tangentially from the nozzle exhaust manifold to cool the nozzle extension. The J-2X, a derivative of the J-2 engine that was used in the upper stages of the Saturn rockets, features a nozzle extension that increases the throat to exit area ratio relative to its predecessor thus creating an engine with a higher specific impulse. The extension walls are designed to be thin to minimize weight; excess weight being increasingly costly for space applications. In order to have these thin walls, the nozzle extension will use film cooling to prevent the structure from failing and buckling due to thermal heat loads, since the existing cooling systems would afford inadequate protection at the nozzle extension. A schematic of the J-2X early in the design process is shown below in Figure 3.

Figure 3. Schematic of the J-2X conceptual design (NASA)

Design of the J-2X and most modern engines are heavily aided by numerical techniques such as Computational Fluid Dynamics (CFD). CFD is used to simulate the fluid processes in J-2X engine operation and also to ensure adequate cooling under realistic operating conditions of a variety of potential designs, which would be difficult to fabricate and test. However simulating all the temporal and spatial scales of the flow using the full Navier-Stokes equations is challenging and impractical for most modern engineering applications. Therefore simplifying models and flow assumptions are used in CFD packages that allow engineering designs to be simulated at the expense of decreasing the level of fidelity of the simulation. In reality, the extent of film protection, which determines the wall temperature, is a function of the complicated interaction of mass, momentum and energy between two physically complicated, shearing turbulent wall-bounded flows. Understanding these interactions and accurately predicting the film's decay using physics-based models is challenging and makes film cooling flows difficult to efficiently design. In addition to the physical film cooling mechanisms, additional three dimensional, design-dependent mixing effects exist as well. Validating and evaluating CFD performance, while generating

film cooling modeling practices is therefore crucial for reliable engine design. These challenges make film cooling the focus of several experimental and numerical studies.

1.1 Background

Two dimensional slot film cooling is commonly used in the combustor liner in gas turbine engines and the thrust chamber assembly, and nozzle in rocket engines. Studying film cooling in canonical configurations, such as the one shown in Figure 4, can aid understanding of the fundamental mixing processes that are responsible for film decay in more physically complicated environments, thus removing factors like three dimensional geometric effects (e.g., injection from discrete holes) from flow effects due to film cooling mixing mechanisms. Figure 4 shows a canonical configuration of tangentially-injected, slot film cooling. The coolant stream is separated from the hot mainstream gas by a louver, or splitter plate. The coolant is then injected into the mainstream. As the coolant advances in the streamwise direction, it mixes with hot, mainstream fluid, and heats up, thus decaying the film and affording less protection of the wall. The mixing process in this flow configuration is heavily
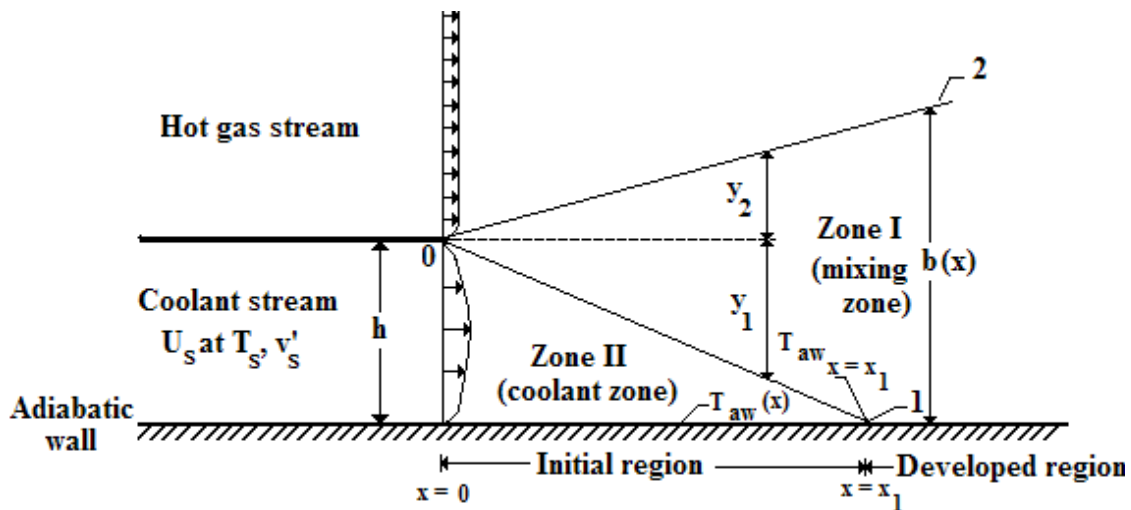
Figure 4. Schematic showing film cooling mixing zones (Adapted from Simon[4])

dominated by the large shear existing between the two turbulent streams.

The relevant design parameter is the wall temperature, which controls whether a material will fail due to thermal loading. The wall temperature in the near injector region, with low radiation and wall heat transfer, assumes a value near the temperature of the coolant fluid adjacent to the wall. The non-dimensional adiabatic wall temperature is the parameter of interest in most research studies. Considering the adiabatic wall temperature, as opposed to the actual wall temperature, separates heat transfer effects due to fluid mixing from those due to temperature gradients in the wall. Therefore what is studied is almost entirely a fluid-mixing phenomenon when radiation, chemistry and other minor effects are ignored. The walls of a rocket engine most likely will not be adiabatic, since most walls have some sort of backside cooling. The heat flux in a non-adiabatic film cooled wall is commonly formulated via a heat transfer coefficient and the adiabatic wall temperature, as opposed to the actual wall temperature.

The primary non-dimensional adiabatic wall temperature of interest is the adiabatic wall effectiveness defined in Eq. (1) as

$$\eta_{ad} = (T_\infty - T_{aw}) / (T_\infty - T_c) \tag{1}$$

where T_{aw}, T_c and T_∞ are the temperatures of the adiabatic wall, the coolant and the hot mainstream, respectively. The effectiveness is unity when the film perfectly protects the wall and is zero downstream when the film and mainstream are fully mixed. The adiabatic wall effectiveness is a non-dimensional parameter that allows differently scaled studies, with different boundary conditions and geometries to be compared.

Similarly, distances are scaled by the coolant injection geometry, which for two dimensional film cooling is the slot height, s.

As stated previously, large shear existing between the coolant and mainstream flows is the primary mechanism of film breakdown. The magnitude of the shear between the two streams is characterized by the velocity ratio, defined in Eq. (2). The blowing ratio, shown in Eq. (3), is a normalized mass flux ratio.

$$VR = \frac{U_C}{U_\infty}$$

(2)

$$BR = \frac{\rho_C U_C}{\rho_\infty U_\infty}$$

(3)

For two-dimensional film cooling, three film mixing categorizations become apparent, depending on the directionality of the shear between the coolant and mainstream. A wall wake is defined to have a velocity ratio lower than unity, meaning the coolant moves slower than the mainstream flow. A wall jet case occurs when the velocity ratio is greater than unity, whereas a minimum shear case is defined by velocity ratios close to unity. The shear causes turbulent Kelvin-Helmholtz vorticies to form, which are responsible for bulk fluid transport and mixing. The wall wake shear vorticies tend to rotate towards the wall. Similarly in a mean mixing sense, the wall wake mixing layer is tilted towards the wall, or said in another way, the mainstream spreads into the coolant. The wall jet shear vorticies are the opposite orientation of the wall wake vorticies, while its mixing layer is oriented away from the wall. In contrast to the other two scenarios, the minimum shear mixing layer has no preferred sense of rotation or tilting of the mixing layer. In most rocket engines where the combustion gasses in the core flow are moving very fast, wall wake mixing is the primary shear scenario. Wall

jets are most commonly found in gas turbine engines, where the exhaust gas moves relatively slowly in the vicinity of the combustor. Each of these regimes have different film break up mechanisms causing the downstream wall temperature, and therefore effectiveness, to evolve differently.

The composition of the coolant and mainstream, upstream turbulence level, boundary layer shape, temperature ratio, compressibility, pressure gradients and Reynolds number upstream of injection have also been identified as factors that alter film mixing and decay[5]. The upstream turbulence level, in both the coolant slot and hot mainstream, influences the enhancement in mixing due to turbulent transport. The Reynolds number and turbulence intensities are historically the most common parameters used in scaling laws to characterize the turbulence in the two streams. The boundary layer shape upstream of injection determines the initial mixing patterns that form between the two streams both in a mean and turbulent sense. In terms of numerical simulations, this implies that properly specifying both the mean and turbulent quantities at the inlet is important. The temperature ratio also influences a variety of mixing parameters including the amount of radiative heat transfer relative to a given reference temperature and the density ratio, which has been shown to affect mixing differently depending on the direction of the shear. Compressibility, which also alters the density ratio, generally acts to suppress turbulent mixing as convective time scales decrease relative to the turbulent mixing scales. The bulk fluid properties are heavily influenced by the composition of the streams, while pressure gradients have variable effects on the film mixing depending on the shear directionality and the sign of the pressure gradient. Geometry effects were not mentioned here, but for slot film

cooling both the angle of injection and the louver thickness to slot height ratio are important. The angle of injection sets the degree to which the film stays attached to the wall at different blowing ratios, while the louver thickness to slot height ratio sets the size of the separation region existing behind the louver lip and the degree of wake shedding off of the louver lip.

Simon[4] highlighted the need for capturing the turbulence information in both streams at the inlet in his semi-empirical, incompressible, zero pressure gradient, wall-jet slot film cooling model. Simon introduced a zonal approach where he divided the film cooling domain into distinct regions or zones. A schematic illustration of these domains is shown in Figure 4, along with other relevant film cooling information. The first region is described as the mixing zone, where both the coolant film and mainstream are mixing causing a rapid decay in the film. The lower boundary of zone I runs from the louver lip to an impingement point along the wall where the "developed region" begins. Zone II is called the coolant zone or the potential core region, where in a mean sense the coolant has not mixed with the mainstream and therefore maintains a high effectiveness at the wall. Simon recognized these two zones were fundamentally different in their composition and mixing patterns, which therefore results in dramatically different effectiveness decays. Before the advent of this model, most analytical methods did a poor job of predicting the near injector field behavior[4]. To better predict the near injector mixing, while also highlighting the importance of properly characterizing the turbulent inlet, the model incorporates both mainstream and coolant turbulence intensities. Simon's model matched experimental data to within 4% for a range of free stream turbulence intensities up to 24% and wall

8

jet blowing ratios up to 1.9[4,6]. For a comprehensive review of previous modeling work, see the work of Goldstein[5]. More recently the work of Dellimore[6] extends the Simon model to incorporate pressure, and density gradient effects.

1.2 Numerical Simulations

The advent of modern computing has allowed CFD to play a key role in the design and analysis of complicated flow paths. With these added resources, engineers and researchers have been able to further explore complicated film cooling flows in hopes of optimizing CFD's accuracy and overall system performance. Direct Numerical Simulation (DNS), Large Eddy Simulation (LES) and Reynolds Averaged Navier-Stokes Simulations (RANS) have been used to numerically tackle film cooling flows depending on the complexity of the problem and the desired fidelity of the results. RANS, which involves temporally averaging the Navier Stokes over a long period of time relative to characteristic turbulent time scales, is considered the lowest fidelity technique. The effect of turbulence is essentially entirely modeled and added to the mean flow quantities. LES involves spatially filtering the Navier-Stokes equations. In this technique, all flow scales greater than the filter width are resolved, while those smaller than the filter width are modeled. Generally, large flow structures that are in nature dependent on the geometry are resolved, while the smaller structures that are more universal and dissipative in nature are modeled. DNS resolve all the relevant flow scales all the way down to the dissipative Kolmogorov scales. No filtering or special treatment is required, but the grid density must be sufficient to resolve gradients on the order of the Kolmogorov scales making grids for most engineering applications very fine. While DNS provides the highest fidelity results, the

numerical grid restrictions makes DNS calculations overly prohibitive for most engineering flows. LES simulations try to balance the level of accuracy with this grid restriction and therefore are more applicable for modern engineering applications. Despite this advantage, LES grid restrictions still are too costly for many complicated engineering designs and analyses, leading to the adoption of RANS in most fluid flow calculations in industry.

1.2.1 RANS Turbulence Models

A variety of different turbulence models have been used to study shear layers, which is the dominant mixing feature in film cooling flows. Wilcox[7] tested and validated many common turbulence models against standard, simple flows to test the accuracy of the RANS approach. Wilcox studied simple free-shear flows, attached boundary layer flows in the presence of pressure gradients and separated flows. Shear flows and attached boundary layer flows are the most relevant flow patterns for tangentially injected film cooling. In these types of flows, Wilcox found that the various turbulence models behave differently depending on the directionality of the shear, e.g. a plane jet or a far wake. For example the Spalart-Allmaras model tends to underpredict wake flow mixing, while overpredicting mixing in jet flows. However the Spalart-Allmaras model does seem to sufficiently capture the mixing for all attached boundary layer flows and free-shear flows, except for jets where the mixing is only moderately captured to within 30%. Wilcox found k-ε models predicted mixing and spreading acceptably for the plane jet case, but were inadequate for the other free-shear flows, attached boundary layers in the presence of pressure gradients and separated flows. The k-ω, on the other hand, performs acceptably in Wilcox's

estimation for all these flows. Wilcox then dismisses shear stress transport models because they are normally predicated on the k-ε model. Additionally, the Baldwin-Lomax model was deemed unacceptable in predicting free-shear flows because tuning of the model coefficients was needed, depending on the shear conditions[7]. Conversely, Pajayakrit and Kind[8] found that the k-ε model, in general, performed well for wall-jet flows but found the k-ω model inaccurately predicts wall-jet velocity profile progression without specific model tuning for the various wall-jet flows.

1.2.2 Numerical RANS Film Cooling Simulations

Early numerical studies featured RANS based computations to predict film cooling flows. Stoll and Staub[9] used a k-ε turbulence model in a parabolic finite difference code to compare simulated wall heat flux values to measurements from their film cooling experiment in a converging-diverging nozzle. A variable turbulent Prandtl number was calculated from an engineering correlation developed for this specific flow. Several supersonic wall wake experiments were simulated, all in the presence of a favorable pressure gradient. The mean coolant inflow velocity profile was generated using a fully developed channel assumption along with a specified mass flux in the coolant channel. The mean mainstream inlet velocity profile was prescribed using an external flow boundary layer assumption along with a specified mass flux in the mainstream without the presence of a cooling slot. The law of the wall was used to recreate the near wall velocity. The turbulence quantities in the mainstream were prescribed according to correlations obtained from previous experimental work in the same facility, while the turbulence quantities in the slot were generated using the fully developed turbulent channel assumption. The simulations captured the wall pressure

very well, while underpredicting the wall heat flux. Other kinematic and thermal data were not reported.

Zhou et al.[10] used a modified k-ε model on a finite-volume code to simulate two dimensional, normally-injected, adiabatic slot film cooling. Using a steady RANS formulation, they simulated two wall wake cases with blowing ratios of 0.2 and 0.4. The turbulent Prandtl number and the thermal governing equation were not reported. The inflow boundary conditions are "precalculated" using a boundary layer flow that closely matches the experimental profiles. For both cases, the mean velocity and turbulent kinetic energy distributions in the film cooling domain show significant deviation from the experimental values. In terms of effectiveness, the authors used the heat and mass transfer analogy to compute heat transfer effects. For the smaller blowing ratio, they found excellent agreement between the simulation and the experiment both in the near injector region and in the far field. The effectiveness differs more dramatically for the higher blowing ratio case. It should be noted that in normally-injected film cooling the primary mechanism of film decay is no longer the shear between the two streams; the extent of film attachment to the wall rather is the primary factor determining the wall protection afforded by normally injected films.

Jansson et al.[11] used both a k-ε model and an algebraic stress model to simulate flat plate slot film cooling for a blowing ratio and velocity ratio close to unity, or minimum shear cases. They performed steady and unsteady simulations of adiabatic film cooling flows for lip thickness to slot height ratios of 0.1 and 1. The turbulent Prandtl number was prescribed between 0.5 and 0.9 depending on the region of the flow. The inlet plane was located two slot heights upstream of the louver lip with the

inlet velocity being prescribed from experimental data. Little large-scale unsteadiness was observed for the smaller lip thickness ratio. The steady results captured the mean velocity and temperature profiles well for this case. For the larger lip thickness ratio, in which large-scale vortex shedding occurred, unsteady RANS calculations were used to resolve the turbulent periodicity in the flow. The mean velocity field was captured fairly well, while the mean temperature field significantly deviated from experimental values especially in the near wall region. The streamwise progression of the adiabatic wall effectiveness was not reported.

More recently, Lakehal[12] used a modified k- ε model that was tuned for jets in crossflow using DNS data to simulate hole film cooling performed by Sinha et al[13]. Lakehal's k- ε model incorporated dynamic coupling with a one-equation model near the wall, anisotropic turbulent transport coefficients and variation of the turbulent Prandtl number based on the local Reynolds number[12]. Models of this nature generally need to be calibrated for the specific flow to perform well. Nonetheless, Lakehal produced very accurate film cooling effectivenesses relative to experiments, both along the hole centerline and laterally outwards for a very complex film cooling flow. For the developing mainstream boundary layer, a $1/7^{th}$ power-law turbulent boundary layer velocity profile was specified along with uniform distributions in k and ε corresponding to the measured mainstream turbulence intensity and dimensionless eddy viscosity ratio. Velocity and flow temperature comparisons were not reported.

Zhang et al.[14] studied liquid film cooling in a rocket combustion chamber using a k-ε model with Van Driest damping near the wall. A plug flow in the film and freestream was specified, while the turbulent inlet information was not reported. They

compared the simulated liquid film length and found their results to be within about 10 percent of experimentally measured values, but provided little other comparisons.

Cruz[15] used the Spalart-Allmaras turbulence model in a finite-difference code to simulate slot film cooling experiments of multiple blowing ratios with both adiabatic and constant temperature walls, which were done by Cruz[15], Raffan[3] and Cruz, and Marshall[16]. In order to create inflow conditions that were consistent with the Spalart-Allmaras model, Cruz[15] developed a precursor simulation method to provide turbulent information for the inlet of a 2D film cooling simulation. For the slot and mainstream flows, a fully developed turbulent channel simulation was run with a characteristic length of the slot height and mainstream boundary layer thickness, respectively. A fully developed turbulent channel profile was fed directly into the film cooling simulations for the coolant flow, while the mainstream profile was modified. Cruz imposed the mean experimental profiles but filtered the turbulent information such that turbulent quantities asymptote to zero in the mainstream. The Spalart-Allmaras model, with a constant turbulent Prandtl number of 0.85, generally captured the adiabatic wall effectiveness well. The mean temperature profiles at different downstream distances were close to experimentally measured values, while the velocity profiles showed some deviation in the far field. Cruz showed that improved accuracy was gained with respect to semi-empirical models developed in other studies. For the adiabatic wall jet case, the validation case for this study, Cruz[15] reports the adiabatic wall effectiveness being within 2% of experimental data. In terms of kinematics, in the far field at x/s of 47.2 the maximum velocity is underpredicted by 22.8%. This large discrepancy was attributed to the constant density assumption used

in the finite difference code and a small entrainment of air into the experimental flow path, which accelerates the flow. For the wall wake and minimum shear cases, the effectiveness remains within 5% and 3% of the experimental data, respectively. In general, the effectiveness showed an initially prolonged ideal effectiveness near the inlet.

Dellimore[17,18] also simulated the adiabatic experiments of Cruz[15] using the Spalart Allmaras model on a finite volume RANS code but ran a series simulations where the constant turbulent Prandtl number ranged from 0.9 to 0.5 to achieve better agreement in the effectiveness and temperature profiles between simulations and the experimental results. These results in general showed an initial prolonged effectiveness of unity and then the effectiveness rapidly decayed. As the turbulent Prandtl number decreases, the turbulent eddy diffusivity increases when the eddy viscosity is held constant, resulting in more thermal mixing. For lower turbulent Prandtl numbers, the length of the potential core was reduced at the expense of increasing the far field decay rate relative to experiments, seemingly indicating that the near field and far field behaviors do not have constant turbulent Prandtl numbers. Dellimore[6], in a later study, developed a high fidelity mainstream precursor simulation method to prescribe inflow turbulence for a blended k-ε, k-ω turbulence model. The precursor simulation involved allowing flow to develop over a flat plate. When the flow field of the precursor simulation resembled the mainstream experimental flow field at the inlet, the simulation was halted. The mean, and turbulent flow quantities were then extracted to input into the inflow of a film cooling simulation. The same slot methodology of Cruz[15] was used for the coolant inflow. Using a constant turbulent

Prandtl number of 0.7, the simulation captured the temperature field to within 2.9% and the momentum field to within 33.1% of the experimental data depending on the velocity ratio that is compared. Dellimore[6] attributed the differences between simulated and experimental results to an experimental leak. This leak Dellimore argued caused a pressure gradient that accelerated or decelerated the fluid depending on the velocity ratio and the region of the flow. The adiabatic wall effectiveness is predicted to within 2.6%, 1.7% and 4.3% of the experimental values for the wall wake, minimum shear and wall jet cases, respectively. Similar to previous RANS studies, the effectiveness decay in the near injector region is underpredicted.

1.2.3 Numerical LES and DNS Film Cooling Simulations

LES and DNS provide higher fidelity CFD solutions since more turbulence scales of the flow are directly simulated, as opposed to the RANS approach where turbulence is completely modeled. Matesanz et al.[19] did one of the first LES and DNS studies of film cooling when they simulated slot film cooling over a flat plate and in a simple converging diverging nozzle using a finite element Navier Stokes CFD code. Their simulations often showed large differences between steady results and instantaneous realizations of the adiabatic wall temperature. In general, their mean results captured experimental values very well, but only limited comparisons were made. Tyagi, and Acharya[20] and Muldoon, and Acharya[21] explored hole film cooling using LES and DNS approaches, respectively. They were successfully able to reproduce important kinematic and thermal flow features, in addition to reproducing velocity and temperature fields very close to experimental values.

Cruz[15] performed a LES simulation of a 2D film cooling wall jet using a constant density, finite difference code. As part of this simulation, Cruz[15] developed a precursor simulation technique to provide time varying inflow conditions that contain realistic boundary layer structures that convect into the film cooling domain. This technique is based off of the methods of Lund et al[22]. This allowed for improved mixing performance near the inlet of the film cooling domain. The effectiveness and temperature profiles produced promising results and were close to experimentally measured values. The peak velocities were underpredicted, which was attributed mostly to the constant density formulation and the experimental leak. To this author's knowledge, this study is the only LES of a 2D film cooling wall jet.

1.3 Experimental Film Cooling Investigation

Due to the complexity of film cooling, there is limited comprehensive experimental data available. Most studies either capture either the turbulent kinematics with limited temperature measurements, or comprehensive temperature measurements with limited kinematic data. Characterizing the velocity, temperature and turbulence upstream of or at the injection plane is crucial for accurate CFD simulations. Additionally, knowing the temperature and velocity profiles, both mean and turbulent, at several downstream locations is important for CFD validation. Cruz[15] and Raffan[3] performed 2D film cooling for the three shear scenarios (i.e. wall jet, minimum shear and wall wake) on an adiabatic and non-adiabatic wall in an open-loop, hot wind tunnel facility. These experiments featured microthermocouple probes and Particle Image Velocimetry (PIV) that provided mean, and root mean squared velocity, and temperature profiles. The wall temperatures, meanwhile, were redundantly captured by

embedded thermocouples and the microthermocouple probes. Using PIV, instantaneous flow structures were captured, showing the coherent turbulent shear structures inherent in these 2D film cooling flows. Additionally, derived skin friction and convective heat transfer coefficients are provided as a function of downstream distance. Unfortunately, while mean inlet velocity and temperature profiles were presented, turbulent quantities were only provided at a short distance downstream of the injection plane. Therefore CFD is required to reconstruct the flow upstream to extract meaningful turbulence information. As noted previously, the test section leaked, which somewhat contaminated downstream velocity profiles. Additionally, the thermal expansion of the louver, which results in a different slot height for each of the shear scenarios, was not accounted for. Despite these deficiencies, this study provided a comprehensive database, allowing for evaluation of CFD performance.

1.4 Objectives

RANS is the standard tool in engineering and industry for simulating film cooling flows, due to the often complex geometry and physics involved, which often makes higher fidelity techniques prohibitive. One objective of this study is to evaluate a NASA based high-speed, fully compressible RANS solver (Loci-CHEM[23-26]) in predicting film cooling performance.

Another goal of this study is to develop engineering modeling practices for tangentially injected, slot film cooling. In film cooling flows, the near injector mixing is of critical importance. Engines are made to replenish the coolant film before it starts dramatically decaying, which Simon associated with the mixing layer impinging on the wall. Therefore, understanding the near injector mixing is crucial to properly

modeling film cooling flows in engineering practice. Far downstream, film cooling flows begin to resemble boundary layers and in these locations experimental correlations capture flow trends fairly well. However this region of the flow is not as critical or difficult to simulate in comparison to the near injector field. Therefore considerable effort and focus will be given to the near injector mixing mechanisms in the experiment and the various computational simulations.

One reason film cooling effectiveness is hard to predict is that there is not enough experimental information to give simulations appropriate inlet boundary conditions. In addition to new comprehensive downstream measurements, new high quality mean and turbulent inlet profiles will be presented using the procedure of Cruz[15] and Raffan[3]. Additionally, very little has been presented in the current literature on the effect of the various assumptions made to create the inflow boundary condition. Towards this end, documenting the results of different inlet techniques in addition to exploring the effect of other common RANS modeling assumptions is a goal of this work. To resolve the discrepancies in the literature, the film cooling performance using various precursor techniques and various turbulence models will be evaluated in a RANS environment. The results are compared to the new experimental and LES values of velocity, temperature, effectiveness and turbulent kinetic energy to gain insight into both the simulated and physical mechanisms that cause film cooling degradation. Since the experimental data has been corrected, definitive comparisons in the absence of the previously noted "experimental leakage" can be made. Building on the insights and findings presented by Dellimore[6,17,18], this thesis will focus on the inlet

behavior and subsequent film cooling performance of several different precursor techniques and inlet treatments in a RANS environment.

Chapter 2: Numerical Methodology and Approach
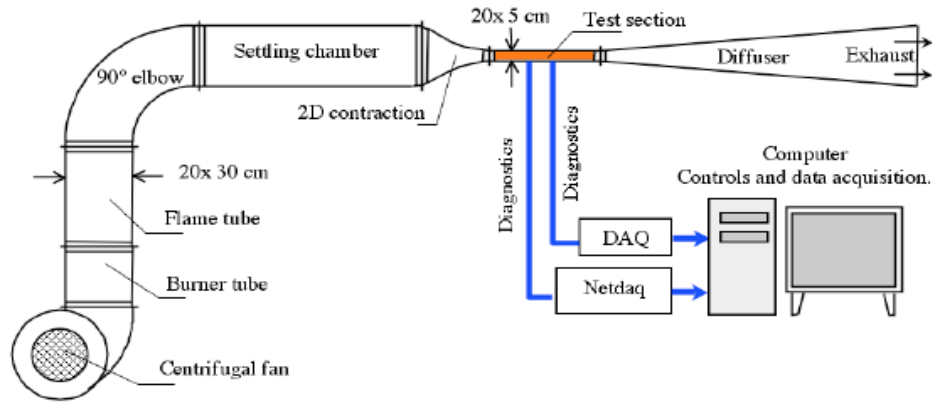
Figure 5. Schematic of hot wind tunnel film cooling facility of Cruz[15] and Raffan[3] used in this thesis for slot film cooling measurements.

2.1 Description of Film Cooling Experiment

The present study numerically simulates subsonic, adiabatic slot film cooling experiments similar to those of Cruz[15] and Raffan[3]. Figure 5 shows a schematic of the experimental facilities that were used to make these measurements. A centrifugal fan, in addition to an exhaust hood, is used to drive the mainstream air. The mainstream flow is pushed through a combustor region, where an inline methane burner is used to achieve the desired temperature ratio relative to the coolant flow. The visciated air then turns 90 degrees through an elbow with turning vanes and then goes through several honeycomb meshes and grids to generate uniform turbulence, destroy boundary layers and smooth the flow. The settling chamber also has a section of randomly oriented ceramic saddles that thermally equilibrate the flow creating a relatively homogenous temperature. After going through the settling chamber, a 2D convergent section with a 6 to 1 contraction ratio is used to further reduce the boundary layer before entering the test section. The coolant is supplied at ambient conditions to a plenum via a high power air compressor. The coolant

air is normally injected from the plenum through small holes into the louver slot. The flow turns in the louver and creates a film that is tangentially injected at ambient conditions via a high power air compressor. The test section consists of the film cooling surface, which is an insulated UDEL® plate with low thermal conductivity, allowing for an approximate adiabatic wall condition to be made. The experimental technique of Cruz[15] and Raffan[3] was used with a repaired test section that had no leakages. Additionally geometric corrections were made to account for thermal growth of the test section and louver, which was previously unaccounted for. Three different slot heights are present for the different velocity ratios (s = 6.06 mm, VR=0.5; s = 5.7 mm, VR=1.0; s = 5.3 mm, VR=1.72) corresponding to the different heating loads on the splitter plate for the three different flows. Particle Image Velocimetry (PIV) is used to capture a full 2-D mapping of both time averaged mean and fluctuating velocities in the film cooling domain. PIV is used to visualize the flow and analyze instantaneous structures. Fast response microthermocouples allow for wall normal profiles of temperature to be measured relatively non-intrusively at multiple streamwise locations. For more experimental details see Cruz[15] and Raffan[3]. New experimental data will be presented for each velocity ratio of the adiabatic film cooling experiment.

2.2 RANS Approach

2.2.1 Details of the Numerical Solver

RANS approaches solve the time or ensemble averaged Navier Stokes equations, providing average flow quantities. Models are used to superimpose fluctuating information on top of the averaged quantities to account for the effect of turbulence on

the mean quantities, most commonly through an extra viscous term. Steady RANS models do not resolve any turbulent scales, rather they are all incorporated in a single model. Loci-CHEM 3.2[23-26], a finite-volume, RANS-based, viscous chemistry solver, was used to simulate the slot film cooling experiments. The governing equations for the mass species, momentum and energy are shown in Eqs. (4-6)[23], respectively.

$$\frac{d}{dt}\int_{CV} \rho_s dV + \int_{dCV} (\rho_s \vec{u} \cdot \vec{n} - \rho_s \vec{V_s} \cdot \vec{n}) dS = \int_{CV} \dot{\omega}_s \, dV$$

(4)

$$\frac{d}{dt}\int_{CV} \rho\vec{u}dV + \int_{dCV}[(\rho\vec{u}\vec{u} + p\vec{I}) \cdot \vec{n} - \vec{\vec{\tau}} \cdot \vec{n}]dS = 0$$

(5)

$$\frac{d}{dt}\int_{CV} \rho e_0 dV + \int_{dCV}[(\rho e_0 + p)\vec{u} \cdot \vec{n} - (\vec{u} \cdot \vec{\vec{\tau}} + \vec{q} + \sum \rho_s h_s \vec{V_s}) \cdot \vec{n}]dS = 0$$

(6)

It should be noted that the primary variables have already been Reynolds averaged. This Reynolds averaging essentially states that the primary variables have been averaged over a long characteristic time scale relative to the turbulent motions, but not necessarily longer than time scales relating to unsteady periodicity, like wake shedding. Using the eddy viscosity assumption, turbulent information is built in through $\vec{\vec{\tau}}$, the shear stress tensor, and $\vec{q}$, the heat flux vector. These quantities include terms with both the molecular, and turbulent viscosity and the molecular, and turbulent thermal diffusivity. The eddy viscosity hypothesis states that the residual stress tensor is proportional to the rate of strain of the averaged velocity; the residual stress tensor being an apparent stress resulting from the averaging of the nonlinear convective flux terms in the momentum equation[27]. The constant of proportionality relating the residual stress tensor and the rate of strain is called the turbulent eddy viscosity. There is an analogous relation for the eddy diffusivity that relates the residual heat flux to the gradient of the temperature field. Eqs. (7-8) show the formulations of the shear stress tensor and the heat flux vector[23].

$$\ddot{\vec{\tau}} = \left(\mu + \mu_t\right)\left(\vec{\nabla u} + \vec{\nabla u}^T\right) - \frac{2}{3}\left[\left(\mu + \mu_t\right)\nabla \bullet \vec{u}\right]\ddot{\vec{\delta}} \qquad (7)$$

$$\vec{q} = \left(k + \mu_t c_p / \mathrm{Pr}_t\right)\nabla T \qquad (8)$$

The turbulent eddy viscosity and eddy diffusivity act in a manner consistent with their molecular equivalents but instead represent the effect of turbulent motion on the mean quantities. Since this problem is underconstrained, additional equations are needed in order to solve for the turbulent eddy viscosity and diffusivity. Most often in RANS based approaches a constant turbulent Prandtl number assumption relates the eddy viscosity and eddy diffusivity, thus reducing the number of equations needed to be solved. Unless noted otherwise a constant turbulent Prandtl number of 0.7 is used for these calculations. Being close to unity, this turbulent Prandtl number approximately satisfies the required, constant turbulent Prandtl number for the Reynolds analogy to hold[10]. The eddy viscosity is found from a turbulence model, which normally involves solving a transport equation for the turbulent kinetic energy and often times a form of the turbulent eddy dissipation, which are then related to the eddy viscosity. For the calculations in this study, the single equation Spalart-Allmaras model[28] (SA), Menter's two equation Shear Stress Transport model (SST) and Menter's two equation Baseline model (BSL)[23,29] were all used to evaluate their performance in predicting film cooling. Loci-CHEM verification studies can be found in Veluri et al[30] and Veluri et al[31]. Validation studies of this code for turbulent, non-reacting flow problems can be found in Dellimore[6].

2.2.2 Boundary Conditions

In engineering calculations, complicated geometry and flow physics require a limited fidelity for economical simulations. Simplified grid domains and artificial boundary conditions are often imposed to alleviate some of these restrictions. For

example, large wind tunnels with a developing boundary layer over a critical face can be approximated as an external flow boundary layer developing over a plate with a zero gradient, wall-normal boundary condition existing in the middle of the wind tunnel, thus creating a reduction in the simulated domain. Other boundary conditions can also be approximately imposed in a similar manner. In general, the inlet conditions must be properly prescribed in order to obtain accurate results over the entire domain. As noted previously, the upstream conditions in both the slot and mainstream flows significantly impact film cooling protection[5]. Therefore the inflow specification should similarly affect film cooling predictions. In practice, inlet conditions must be generated due to insufficient data at the inflow plane, which will introduce errors into a film cooling simulation due to inaccurate specification. To better understand these errors, multiple inlet treatments and film cooling grid domains are used to explore the effect of these simplifications.

2.2.2.1 RANS Film Cooling Boundary Conditions

Figure 6 shows a schematic of the 2D film cooling problem considered in this study. A splitter plate or louver separates the hot mainstream and slot coolant flows. The coolant is injected tangentially along a flat plate, insulating the wall from the higher temperature mainstream
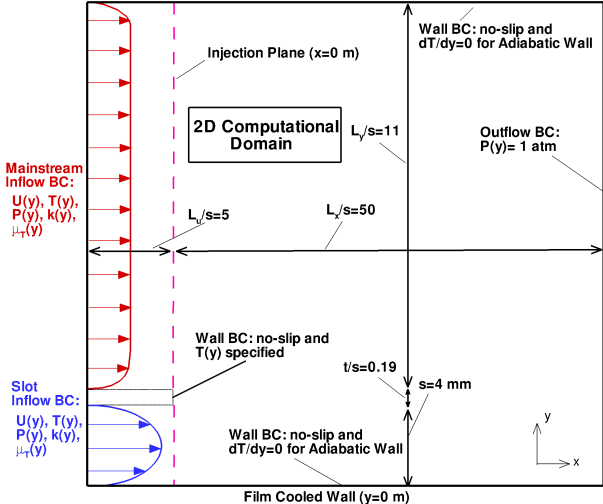
Figure 6. **Schematic of the film cooling simulation with boundary conditions and grid dimensions listed.**

flow. The extent of the film is governed by the complicated turbulent mixing of these two flows downstream of injection. A shear layer, which defines the extent of mean mixing, develops at the interface of the two streams just past the injection plane and is a dominant mechanism of 2D, tangentially injected, slot film cooling decay.

The schematic shows the numerical simulation boundary conditions and dimensions for a typical film cooling domain used in this study. The thick black line on the perimeter defines the extent of the domain simulated. Additionally note that the inflow plane is not in this case coincident with the injection plane (the streamwise plane where the two streams start mixing). In all the RANS simulations in this thesis, heat transfer through the solid louver is not considered, however the temperature at the louver wall is specified. The two wind tunnel walls impose no slip and adiabatic boundary conditions, meaning both the velocity and wall normal temperature gradient go to zero at the wall. The outflow boundary condition features a subsonic characteristic based condition that enforces constant pressure at the outflow plane. Since pressure does not vary too much in the wall normal direction for the category of flows considered in this study, this assumption was deemed acceptable. The spanwise boundaries use symmetry boundary conditions. Additionally thermal radiation effects are ignored.

Prescribing inlet conditions requires some care and varies depending on where the inlet is defined. Since turbulent inlet data was not available for all the inlets, precursor simulations were performed to generate physically meaningful turbulent information. Turbulent quantities such as the eddy dissipation are difficult parameters to experimentally measure, since they involve turbulence at the small viscous length scales, thus leading to a slight inadequacy of most detailed data sets for use in RANS and LES

computations. The mean profile of the primary variables at the inlet of a film cooling simulation can either be specified from experimental data or can be developed from the precursor simulation based only off of key parameters of the flow, like the mass flux and flow temperature. The latter is adopted for most of the cases in this study, due to the fact that experimental data does not exist upstream of the injection plane, nor will such profiles exist in many engineering applications.

2.2.2.2 Film Cooling Inlet Location and Grid

Three different film cooling domains were used to test the effect of the inlet plane location; more specifically the relative location of the inlet plane in regards to the injection plane. The first two grids prescribe inflow conditions on the injection plane (regular grid) and five slot heights upstream of the injection plane (upstream grid), respectively. It should be noted that the schematic seen in Figure 6 is an example of an "upstream grid". One would expect the location of the inlet plane would need to be sufficiently removed from the injection plane due to pressure and flow disturbances occurring in the separated region existing just behind the splitter plate. Since this is subsonic flow, flow characteristics can propagate upstream and therefore affect the flow. For the low speed subsonic flows and scales being considered in this study, these disturbances should be relatively small, so five slot heights was deemed to be sufficient to capture all relevant physics. Additionally, CFD codes often require a dirichlet pressure boundary condition at the inlet. When this occurs with a "regular grid", the pressure boundary condition will no longer be approximately constant in the wall normal direction due to the low pressure region existing behind the louver. No obvious boundary condition exists for the pressure. Therefore, if a constant pressure boundary is enforced the flow

will adjust to the pressure, essentially changing the inflow boundary condition. The last grid (called the fully coupled grid) is a film cooling domain that incorporates both the wind tunnel geometry far upstream of the injection plane and the experimental test section. This last grid provides the highest accuracy as there are no errors from decoupling the precursor simulation and the film cooling simulation.

Three grids each with different inlet locations were used to simulate this pseudo 2D slot film cooling for the wall jet case. The "fully coupled" grid was the only grid used for the other velocity ratios. The "regular" or baseline grid contains only the film cooling mixing region, starting at the injection plane and ending at the exit plane, see Fig. 6. This region extends 200 cm or roughly 40 slot heights (i.e., $L_x \sim 40$ s) in the streamwise direction, 48 mm in the wall normal direction corresponding to approximately 10 slot heights (i.e., $L_y \sim 10$ s) and 1 mm in the spanwise direction or roughly 1/5 of a slot height (i.e., $L_z \sim 0.2$ s). Since this film cooling process and all simulated boundary layers are two dimensional in the RANS framework, this small domain length in the spanwise direction was deemed sufficient. Since turbulent structures are not actually resolved, but modeled from the mean quantities, this pseudo 2D assumption is valid. The "upstream" film cooling grid, which is shown in Fig. 6, includes this film cooling mixing region but also extends five slot heights upstream of the injection. The "fully coupled" film cooling grid attaches a slot precursor and a mainstream precursor domain to the film cooling mixing domain. Resolving velocity and temperature gradients in the viscous sublayer near the wall and in the shear region is of critical importance for boundary layer, convection heat transfer problems. For all grids considered, the first grid point was less than 1 wall unit (i.e., $y^+ < 1$) from the wall in the wall normal direction, where the wall

normal distance is normalized by the frictional length. The wall fricitional velocity and frictional length are defined in Equations 9 and 10[26], and are important considerations when defining grid spacing in viscous flows.

$$u_\tau = \sqrt{\nu \frac{\partial \overline{U}}{\partial y}}\Bigg|_{y=0}$$

(9)

$$\delta_\tau = \nu / u_\tau$$

(10)

The overbar refers to time averaging of the velocity field, while the velocity gradient is evaluated at the wall. On average the wall normal spacing at the wall was approximately 0.1 wall units (i.e., $y^+=0.1$). To ensure adequate spacing and grid density was observed, grid independence studies were performed on each film cooling and precursor grid. Four grid resolutions were considered and once the results between subsequent grids were invariant to within less than 0.1% in terms of the adiabatic wall effectiveness, velocity and temperature, the grid was deemed grid independent, which ensures finer grid resolution would not yield more accurate results. The regular, upstream and fully coupled film cooling grids for each velocity ratio case consist of approximately 132,000, 156,000 and 412,471 cells, respectively. Global residuals and local properties at several stations were monitored until converged, steady solutions were reached.

2.2.2.3 Slot Inflow Generation

Now that the inlets of the grids have been defined, the inflow boundary conditions can be discussed. As was used by Cruz[15] and Dellimore[6], a fully developed turbulence assumption was made for the
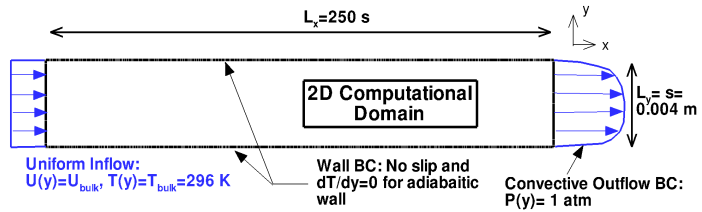
Figure 7. **Schematic of the Fully Developed Turbulent Channel Slot Precursor Simulation.**

coolant flow. Figure 7 presents a schematic of the slot precursor simulation with numerical boundary conditions and dimensions listed. The precursor domain has a channel length of 250 slot heights in the streamwise direction. The development region for turbulent channel flows is typically shorter than the laminar developing region and often times dramatically so. The turbulent entry length for turbulent flows is on the order of 10 diameters as opposed to 100 diameters for laminar flow in circular tubes[32]. For this precursor simulation, no slip, adiabatic conditions are applied at the walls while a constant pressure outflow boundary conditon is prescribed at the exit. The mass flow rate is prescribed at the inlet and the boundary layer is allowed to develop until fully developed turbulence is reached, meaning time averaged quantities no longer vary in the streamwise direction. Another way of thinking about this is that the mean wall shear stress is constant. The turbulent information can then be extracted at the exit plane of the simulation or five slot heights upstream of the exit plane, depending on the film cooling grid that is used (e.g., regular or upstream grid). This information is then fed into the appropriate film cooling simulation. For the fully coupled grid, this precursor simulation is directly coupled to the film cooling domain, i.e. the film cooling domain includes the precursor simulation domain.

2.2.2.4 Mainstream Inflow Generation

The hot mainstream flow more closely resembles a developing boundary layer, spatially evolving in the streamwise direction. Three inlet generation strategies were used to model the hot mainstream flow upstream of injection. Figure 8 shows schematics of the different mainstream precursor simulations with numerical boundary conditions and dimensions listed.

2.2.2.4.1 *Fully Developed Turbulent Channel*

The first method, adopted by Cruz[15] and shown in Fig. 8a, involves simulating only the boundary layer on top of the splitter plate. A fully developed turbulent channel is once again assumed, with the channel height being twice the boundary layer thickness, defined as the height at which the flow velocity is 99% of the freestream value. When considering only the bottom half of a fully developed turbulent boundary layer in a channel, it resembles the boundary layer shape of an external flow at a single streamwise location, developing over a flat plate. The fully developed turbulent profile can be artificially filtered, using a hyperbolic

a)

$L_x=250\ \delta_{99}$

y
x

2D Computational Domain

$L_y=2\ \delta_{99}=$ 0.00632 m

Uniform Inflow:
$U(y)=U_{main}$, $T(y)=T_{main}=462$ K

Wall BC: No slip and dT/dy=0 for adiabaitic wall

Convective Outflow BC: P(y)= 1 atm

b)

Freestream BC:
dT/dy=0, du/dy=0

d=0.1 m

$L_x=8.5\ d$

Wall BC: No slip and $T_{wall}=307$ K

d/100

$L_y=10\ d$

Outflow BC:
P(y)=1 atm

Uniform Inflow:
$U(y)=U_{main}$,
$T(y)=T_{main}=462$ K

Freestream BC:
dT/dy=0, du/dy=0

y
x

c)

$L_x=6$ in= 0.1524 m

Wall BC: No slip and dT/dy=0 for adiabatic wall

2D Computational Domain

$L_y=10\ s =$ 0.040 m

Uniform Inflow:
$U(y)=U_{main}$, $T(y)=T_{main}=462$ K

Wall BC: No slip and $T_{wall}=$ 307 K

Convective Outflow BC: P(y)= 1 atm

Figure 8. **Schematic of the mainstream precursor simulation techniques, featuring a) fully developed turbulent channel, b) flat plate and c) wind tunnel simulations.**

tangent function, to create flow profiles that asymptote to mainstream values. Once filtered, the turbulent information can then be prescribed at the injection plane since this is where the boundary layer is described in the experiment. Further details of this technique can be found in Cruz[15]. Since the boundary layer thickness will change depending on the upstream location, this technique can only be used on film cooling grids with inflow planes coincident with the injection plane, unless the boundary layer thickness is known upstream of the injection plane. The rationale of this approach is that the majority of the turbulence is contained in the boundary layer for most turbulent flows. Thus if the turbulence in the boundary layer is approximated correctly, the mixing should closely resemble higher fidelity approaches.

The mass flux is not prescribed from experimental values. The mass flux going into this fully developed turbulent channel simulation is varied over a series of simulations until non-dimensionally the boundary layer shape (e.g., velocity normalized by the mainstream velocity vs. the wall normal direction normalized by the slot height) resembles the experimental boundary layer, in terms of the displacement thickness and the momentum thickness. To understand why this mass flux variation is necessary relative to the experimentally derived mass flux, consider a developing boundary layer in a channel starting from plug flow. Initially, the wall gradients near the wall will be very high, since the disturbance created by the wall has not been allowed to diffuse into the flow. As the flow develops, the disturbances created by the wall propagate into the flow and the gradients at the wall become less steep. Eventually a fully developed region is reached where the gradients become their smallest at the wall and where all of the flow feels the effect of both walls. Since the experimental mainstream flow is still developing,

the gradients at the wall will be steeper than a fully developed turbulent channel calculation meaning the mass flux for this fully developed turbulent channel flow must be increased to achieve similar gradients and boundary layer shapes. This artificial parametric variation of the mass flux is a hindrance of this technique. Additionally detailed information on the boundary layer shape is required.

Another major flaw of this technique is the ambiguity of the temperature boundary conditions. The mainstream wall ,due to heat transfer through the louver into the coolant, will be at a lower temperature than the hot mainstream flow. However the upper boundary in this fully developed turbulent channel simulation is two full boundary layer thicknesses into the mainstream flow in the wall normal direction, so no simple specification is apparent. In this study adiabatic walls were used in the precursor simulation, while the experimental temperature profile was specified at the film cooling inlet, thus alleviating this ambiguity somewhat. Once again, symmetry boundary conditions are used on the side walls, while the out flow boundary condition features the same constant pressure boundary condition used previously.

2.2.2.4.2 Flat Plate Simulation

The second method, used by Dellimore and shown in Fig. 8b, involves simulating the mainstream as a boundary layer developing over a flat plate[3]. Developing profiles are extracted at a streamwise location where they resemble the mean experimental injection plane conditions, and not at a previously determined, physically significant, geometric length. For the upstream grid, inlet profiles from the mainstream precursor simulation should be extracted five slot heights upstream of this previously determined streamwise extraction location (i.e., the location where the simulation velocities resemble the

33

mainstream experimental velocities at the injection plane). In this method, a no-slip condition and the louver wall temperature are prescribed at the wall. The louver wall temperature is estimated from the first experimental film cooling temperature profile approximately 0.5 slot heights downstream of injection. The outflow once again features the constant pressure boundary condition. The top and bottom boundaries are far field boundary conditions that impose a zero wall-normal gradient in the primary variables. At the inflow, the experimental bulk mainstream velocity and temperature are prescribed. It can shown that the ambiguity in the temperature wall boundary condition is now resolved, since the thermal boundary condition can be allowed to develop in a physically meaningful way. This simulation technique does, however, still require specific knowledge of the flow profiles at the injection plane.

2.2.2.4.3 Wind Tunnel Simulation

The last precursor approach, shown in Fig. 8c, models the actual wind tunnel hardware in the mainstream, starting at the exit of a converging nozzle and ending at the film cooling injection plane. Experimentally, the converging nozzle was used to destroy the boundary layer existing upstream. For the present study, flow exiting the nozzle, or entering this precursor simulation, was assumed to be plug flow, since the boundary layer height is very small. In this method, a no-slip condition and the louver wall temperature are prescribed at the louver wall. The outflow once again features the constant pressure boundary condition, while the side walls are symmetric boundary coniditions. The top boundary is assumed to be adiabatic and have zero slip at the wall. At the inflow, plug flow with the experimental bulk mainstream velocity and temperature is prescribed. Once again profiles can be extracted at the exit plane or five slot heights upstream of the

injection plane depending on the film cooling grid being used. For the fully coupled grid, this mainstream wind tunnel domain is directly attached to the film cooling domain. Since velocity, temperature, turbulence information and pressure must be prescribed at the inflow plane, this last technique also has the added advantage of maintaining the correct pressure development with respect to the injection plane. Flat plate external flows, for example, experience very little changes in pressure as flow spatially develops. A large wind tunnel will also have a different pressure evolution than a fully developed turbulent channel, as is assumed using the first mainstream precursor method. When the streamwise pressure progression is not consistently preserved and no pressure is measured, the pressure at the inlet of a film cooling domain must be artificially iterated until rapid gradients and unphysical flow development no longer appear over the first few grid cells.

2.2.3 Parametric Space Explored

Three different turbulence models were also used in the film cooling simulations. The baseline turbulent method used was Menter's two equation shear-stress transport (SST) model[28]. The SST model is a blended k-ε, k-ω model. k-ε models suffer instabilities when encountering large separation of turbulent

Table 1. Summary of experimental conditions explored in this paper.

VR	U_∞ (m/s)	U_c (m/s)	T_∞ (K)	T_c (K)
1.72	11.15	19.21	464.85	294.04
0.86	21.08	18.04	455.15	286.13
0.45	25.07	11.19	463.24	295.07

Table 2. Summary of independent parameters explored.

Film Cooling Grid	Mainstream Precursor Simulation	Turbulence Model	RANS Averaging
Regular	Fully Developed Turbulent Channel	SST	Time
Upstream	Flat Plate Boundary Layer	BSL	Ensemble
Fully Coupled	Wind Tunnel Simulation	SA	

time scales and uses damping functions near the wall to resolve the viscous sublayer. The k-ω model requires no damping functions to resolve the viscous sublayer, but has difficulty capturing free shear flows correctly[21]. Therefore, a blended k-ε, k-ω model should feature a k-ω formulation near the wall and should transition to a k-ε formulation away from it. The SST model was derived from Menter's Baseline (BSL) model[28], which is also used in this study. The SST has a slightly different formulation of the eddy viscosity in that it considers the vorticity[21]. The last turbulence method explored is the one equation Spalart-Allmaras (SA) model[27]. In this model, a modified eddy viscosity is solved for directly, as opposed to most two equation models, which use equations for the turbulent kinetic energy and a dissipation term, to construct the eddy viscosity. The reader is referred to Menter[21,28] and Spalart, and Allmaras[27] for more information on these turbulence models. Both steady-state RANS and unsteady RANS (URANS) solutions were considered, URANS being capable of capturing large-scale periodic turbulence, like vortex shedding from the louver lip.

Three experiments with different velocity ratios corresponding to the corrected experimental results of Cruz[15] were simulated in this paper and are summarized in Table 1. The full parametric space was only explored for the wall jet, or velocity ratio of 1.72, case. The best practices for the wall jet case were then applied to the wall wake (VR = 0.44) and minimum shear (VR = 0.86) simulations. Table 2 shows the parametric space that was explored as part of this study. Parameters were varied independently defining a large test matrix. In the interest of space, only noteworthy or meaningful results are shown, while other results are briefly mentioned. Since performance was shown to vary depending on the shear scenario for a given turbulence model, each turbulence model was

used to simulate film cooling in each shear regime. Once again, three different grids were used for the wall jet case corresponding to the inlet placement in relation to the injection plane. The mainstream precursor simulations explored for the wall jet case are the fully developed turbulent channel simulation (FDTC), the flat plate boundary layer simulation (FPS) and the wind tunnel simulation, as was discussed previously. Unless noted otherwise, the SST model was used for all parametric studies involving the film cooling grid or precursor simulation used.

2.3 LES Details

To gain further insight into RANS turbulence modeling and the physical mechanisms that are resolved, an LES of wall jet film cooling was run for comparison. LES codes calculate higher detailed turbulent mixing. LES3d-mp developed by Anthony Keating[33] is used to simulate the 2D wall jet, adiabatic slot film cooling experiment. The details of LES3d-mp, the numerical methodology and the numerical procedure can be found in Cruz[15]. Further verification and validation studies can be found in Keating[33]. LES3d-mp is a low speed, finite different code that is 3rd order accurate in time and 2nd order accurate in space. It also features the dynamic procedure for calculating the turbulent eddy viscosity and turbulent eddy diffusivity for the kinematic and scalar fields, respectively. This turbulent formulation allows for variable turbulent Prandtl numbers. The temperature or energy equation was assumed to be a passive scalar in this code formulation, meaning variable density or viscosity is not considered. All that was changed for this simulation relative to that of Cruz[15] was the modified boundary conditions, incorporating the new slot height, grid domain and the slightly different

inflow conditions. When comparing to the present grids, the film cooling domain used in this simulation would be deemed a "regular" grid, or a grid where the inflow plane is coincident with the injection plane.

The LES precursor simulation features fully developed turbulent channel calculations for both the mainstream and slot. The actual computational methodology used for this simulation is different from that of the RANS fully developed turbulent channels calculated above. The major difference is that periodic boundary conditions are used on the streamwise inlet and exit, meaning that the flow exiting the channel is fed in as the inlet to the channel. In this way, one can imagine they are riding along a control volume that moves with the average velocity of the fluid in the channel. As the control volume moves downstream, the fluid spatially develops and eventually reaches fully developed turbulence. In order to offset difference in momentum flux entering the channel versus exiting, a mean pressure gradient term must be added to the governing equations to keep the momentum constant. This mean pressure gradient, as in the actual physical scenario, is present in order to overcome friction at the wall retarding the fluid. Another major difference getween the LES and RANS simulations is that the turbulent structures in LES calculations are resolved, so all calculations are three dimensional and time varying. All subsequent LES results shown have been averaged taking into account these complexities.

The LES film cooling simulation and the previously discussed RANS simulations use a Prandtl number of 0.71. The LES grid has 256, 152 and 64 points in the streamwise, wall-normal and spanwise directions, respectively. This corresponds to spacing ranging from 43 to 58 and 14 to 19 in wall units in the streamwise and spanwise directions,

respectively. The wall normal spacing at the wall ranges from 0.49 to 0.67 in wall units. These spacings are representative of LES spacings used in channel flows as given by Piomelli[34] and Chapman[35].

2.4 Precursor Methods Modeling Summary

Table 3 shows a summary of the different modeling assumptions and specifications inherent to the different precursor techniques. As was previously discussed, the mainstream fully developed turbulent channel calculation requires the most limiting assumptions. For this technique, velocity and temperature are artificially imposed at the film cooling inlet, with the thermal boundary layer not being incorporated or resolved. The turbulence parameters in the boundary layer are calculated however, which fulfills the need for turbulent specification at the inlet of a film cooling simulation. However detailed mean experimental measurements are needed at the inlet. Pressure still needs to be iterated at the film cooling inlet. Additionally this technique can not be used on a grid with an inlet upstream of the film cooling injection plane, since it requires experimental data calculated in the film cooling domain. The mass flux going through the channel is artificially varied to best match the experimental non-dimensional boundary layer inlet shape in the mainstream. As is the case for most RANS simulations, the turbulent kinetic

Table 3. Modeling Assumptions and Specifications are shown for the different precursor simulation techniques.

Modeling Specifications						
Simulation Type	RANS	RANS	RANS	RANS	LES	LES
Inlet Region	Slot	Mainstream	Mainstream	Mainstream	Slot	Mainstream
Precursor Type	FDTC	FDTC	FPS	Wind Tunnel	FDTC	FDTC
Velocity Filtered at FC Inlet		X				X
Temperature Imposed at FC Inlet		X			X	X
TKE is used in simulation	X	X	X	X		
Wall Thermal Boundary Condition	Adiabatic	Adiabatic	Wall Temperature	Wall Temperature	Adiabatic	Zero Scalar at Wall
Pressure Iterated at FC Inlet		X	X			
Turbulent Prandtl Number is Constant	X	X	X	X		
Usable with Upstream Grid	X		X	X		
Artificial Mass Flux		X				X

energy is modeled and a constant turbulent Prandtl number is specified. The mainstream flat plate simulation also has a number of modeling assumptions and restrictions, while the slot fully developed turbulent channel and mainstream wind tunnel simulation have the least, meaning they require the least amount of artificial processing and most closely match the physics of the experiment.

Chapter 3: Results

The focus of this chapter is to present the results of the numerical adiabatic film cooling simulations, both LES and RANS, and compare them to corrected experimental data in the hope of understanding the agreement and inherent inaccuracies of these simulations. All three shear scenarios are explored, but the majority of the parametric studies focus on the wall jet simulation, where both RANS and LES simulations have been performed. The practices and insights gained from the wall jet simulations are then applied to simulating the minimum shear and wall wake cases.

3.1 Wall Jet Case

3.1.1 Precursor Results

As Goldstein noted[6], film cooling performance strongly depends on the kinematic and thermal states upstream of injection. Due to often limited data available to quantify the upstream state in engineering applications, a variety of precursor simulations were studied in order to determine their accuracy, ease of use and applicability to film cooling. The important near injector mixing should especially be affected by the initial state of the coolant and mainstream.
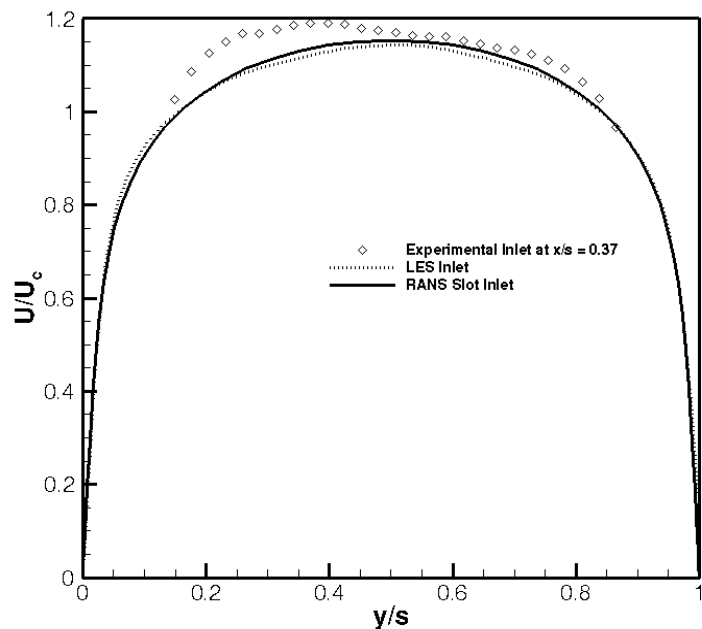

Figure 9. Comparison of wall jet inlet slot velocity profiles.

Figure 9 shows the inlet velocity profiles in the slot region of the adiabatic wall jet film cooling experiment described previously and the RANS, and LES precursor simulations. The kinematic experimental inlet is actually taken 0.37 slot heights downstream of injection. The RANS precursor simulations shown here use the SST turbulence model. The LES and RANS curves provide similar estimates for the mean velocity profiles, which is not surprising since turbulence models are often validated against simple canonical studies such as flow through a channel. The LES curve estimates a slightly flatter velocity curve, with a slightly higher shear stress at the wall.

The experimental data is seemingly missing data near both the slot walls. This experimental data is unrecoverable near the wall due to laser reflections and wall noise in the PIV measurements. In PIV applications, walls tend to reflect more light than seeding particles in the near wall region and therefore drown out the cross correlation of the particles near the wall. The experimental data has therefore been truncated near the wall to provide only data that is physically meaningful. Notice that the kinematic quantities are most often normalized by the bulk coolant velocity, or the average velocity in the channel. Since there is data drop out near the wall, this average should be affected and will not represent a true mean of the coolant velocity. In order to overcome this deficiency, a cubic spline technique was used to reconstruct the near wall velocity using the no slip condition at the wall and the continuity of velocity and its first, and second wall normal derivatives of velocity at the first valid experimental data point above the wall. This technique was tested on a fully developed turbulent channel RANS simulation that was truncated at a similar wall normal location as the experimental data. The cubic splines technique provided a marked improvement over

simply ignoring the near wall area or assuming a linear fit in the data drop out region. The bulk velocity of the truncated RANS curve with the cubic spline matched to within 0.05% of the entire resolved RANS curve. While the computational and experimental velocity curves are close, the bulk velocity does still seem to be slightly underpredicted since the non-dimensionalized velocity seems to sit on top of the computational curves.

Figure 10 shows the inlet velocity profiles for the different RANS precursor simulations, the LES simulation and experimental data near the injection plane. The experimental curve once again shows data drop out above the top of the splitter plate. The RANS and LES fully developed turbulent channel simulations for the mainstream are very close to the experimental curve, which is not surprising since the mass flux in the channel was adjusted until the velocity profiles of the simulations non-dimensionally matched that of experiment. The profile from the top of the mainstream fully developed channel calculation has been artificially filtered so that the velocity assumes the mainstream value at the channel half height, or the boundary layer thickness. The boundary layer thickness from the wind tunnel simulation is thicker and has a smaller wall shear stress than the experiment.
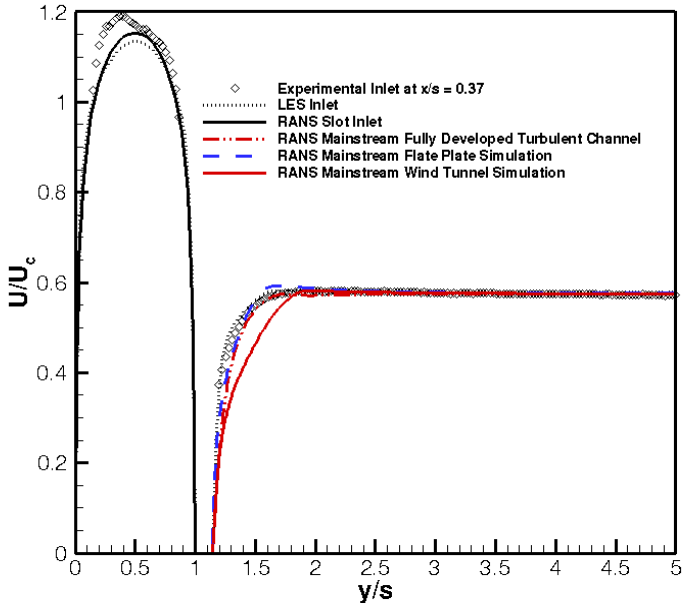

Figure 10. Comparison of wall jet inlet velocity profiles.

43

The streamwise progression of velocity in this RANS simulation clearly differs from that of the experiment, which it is trying to directly simulate. In part, this discrepancy can be attributed to the lack of turbulence prescribed at the inlet of simulation. Higher turbulent kinetic energy will make the boundary layer more turbulent making the shear stress at the wall higher and more in line with the experimental trend. The flat plate simulation has a slight bulge in the boundary layer. This bulge is typical of flow in the entrance region of a pipe or channel. Overall the flat plate simulation matches the boundary layer shape very well, which is not surprising due to the fact that the extraction location in this precursor simulation occurs where the boundary layer resembles the inlet mainstream boundary layer.

The slot turbulent kinetic energy at the inlet can be seen for the experimental data and the fully developed turbulent channel precursor simulations in Figure 11. It should be noted that the experimental data is actually measured slightly downstream of injection at x/s of 0.37, due to noise issues near the louver. Goldstein notes that the turbulence level in the slot impacts the film cooling protection[6]. Since the experiments and LES only
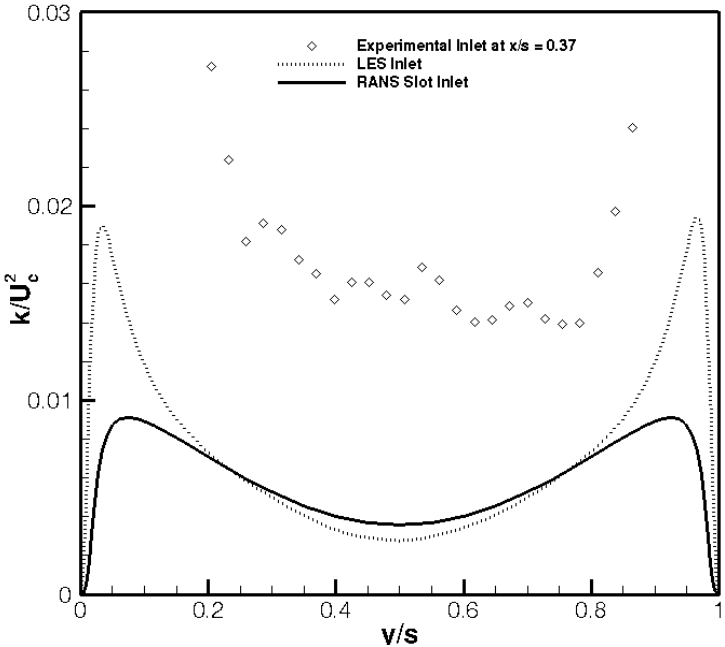

Figure 11. Comparison of wall jet inlet slot turbulent kinetic energy profiles.

44

resolve the flow down to a certain scale, the turbulent kinetic energy from sub-resolved and subgrid scales are not accounted for. However, turbulent theory dictates that the large-scale eddies contain the majority of the flow's energy and should, therefore, account for almost all of the turbulent kinetic energy. Thus, the turbulent kinetic energy curves are well resolved by the simulation and experiment. Additionally, the experimental data set does not measure the spanwise direction of velocity, so this velocity component was neglected in these turbulent kinetic energy results. Both computations predict vastly different turbulent kinetic energies than the experimentally measured quantities. The RANS curve provides the lowest estimate of turbulent kinetic energy overall, with the peak turbulent kinetic energy in the RANS simulation being only 53% of the peak LES turbulent kinetic energy. The RANS curve also has a fundamentally different shape than the LES curve in the sense that the trough divided by the peak of the turbulent kinetic energy is greater for the RANS curve. This shows that the turbulence mechanisms are somewhat different. The LES simulation predicts peaks in turbulent kinetic energy closer to the wall than the RANS simulation does, while both simulations dramatically underpredict the turbulent kinetic energy relative to the experimentally measured values. The second order statistics of the LES code have been validated with respect to DNS data of a fully developed turbulent channel at similar Reynolds number, so the LES curve should be representative of a fully developed turbulent channel. The discrepancy between the simulations and experimental data can therefore suggest two things. First the slot flow may not be well represented by the fully developed turbulence assumption. Alternatively, the second order statistics on the experimental data may have not fully

45

converged due to either insufficient samples or data dropout in this near injector region where wall reflections off the film cooled wall and splitter plate create noise issues. The jaggedness in the experimental data curve seems to suggest the latter. Modelers should be wary of experimentally measured values of turbulent kinetic energy provided near walls. These profiles are not often provided exactly at the inlet location due to these wall noise restrictions. Additionally, the turbulent kinetic energy profiles can change rapidly, especially in the near injector region of a film cooling experiment. The differences in the computational turbulent kinetic energies suggest more vigorous mixing will occur in the slot inlet region of the LES film cooling simulation than that of the RANS. The progression of turbulent kinetic energy will be explored later on and more definitive conclusions can then be drawn.

Figure 12 shows a comparison of the turbulent kinetic energy for the experiment slightly downstream of injection and the different precursor simulations at the injection plane. Once again, the experimental data was derived from turbulent kinematic information prescribed 0.37 slot heights downstream of the injection plane, meaning the slot flow has already started expanding and interacting with the mainstream boundary layer slightly distorting the turbulent
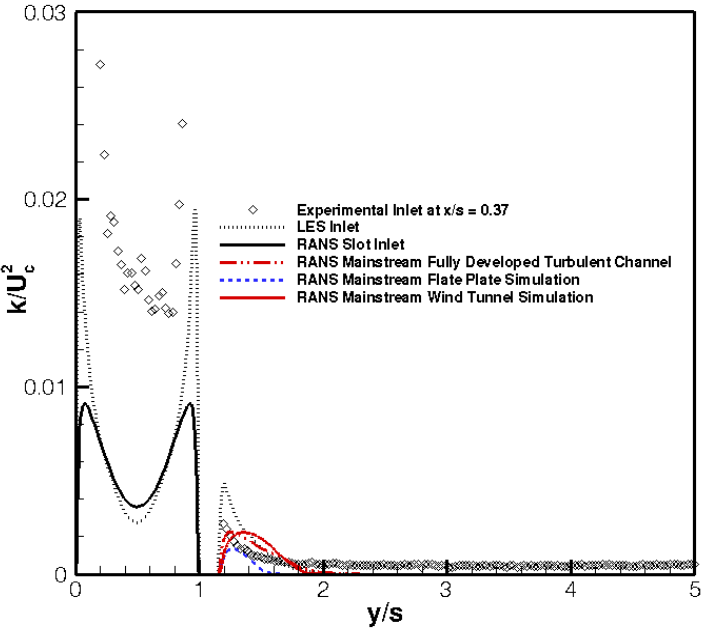
Figure 12. Comparison of inlet turbulent kinetic energy profiles for the wall jet case.

46

kinetic energy. The turbulent kinetic energy peak near the cooled wall, however, should remain close to its actual state at the injection plane, since the flow near the wall, at least initially, should not encounter mainstream structures. The experimental results do not fully capture the peak near the wall due to the inherent noise issues associated with PIV near solid boundaries. The data is truncated to the first valid data point occurring near the peak in the turbulent kinetic energy. The mainstream turbulent kinetic energy seems to be over predicted by the LES simulation and slightly under predicted by the RANS simulation but both remain close to the experimental mainstream values. The flat plate precursor simulation provides the lowest estimate of turbulent kinetic energy, but in general all the curves are of the same order of magnitude in the mainstream. The values of the mainstream curves are well below that of the coolant flow, which is expected since the coolant is moving much faster and is therefore more turbulent. It should be noted that the actual peak in the turbulent kinetic energy in the mainstream may actually have been filtered out and may exist between the top of the slot and the bottom of the mainstream, since the experimental location is slightly downstream of injection. The mainstream is partially mixed at this point causing the turbulent kinetic energy peak to move into the separation region. The actual mainstream turbulent kinetic energy peak is therefore unknown, since wall noise is still prevalent in this region. The turbulent kinetic energy shapes of the different precursor simulations slightly differ from that of the experiment, but since they all have slightly different treatments, this is not unexpected. Also all precursor simulations asymptote to zero turbulent kinetic energy, while the experiment has a small, finite value, showing there is some residual turbulence in the wind tunnel at the

47

exit of the converging nozzle all the way into the experimental test section. Recall, this residual turbulence is a possible explanation for why there are discrepancies between the velocity boundary layer of the experiment and the mainstream wind tunnel simulation.

The inlet temperature profiles are shown in Figure 13. The thin vertical dash lines represent the location of the louver in wall normal space. A simple linear gradient is prescribed in this region for all cases. Notice that the experimental data is once again taken slightly downstream of the injection plane at x/s of 0.51. Here the temperature profile has mixed slightly already so the actual experimental temperature at the inlet will be different, especially near the louver. Note that the only reason the mainstream temperature profiles between the RANS and LES fully developed turbulent profiles are different is because the imposed profiles were not the same. There is nothing physical in this difference, however. The flat plate simulation provides an inlet temperature profile that is similar to the RANS mainstream fully developed turbulent channel profile. Consistent with the kinematic results, the wind tunnel simulation predicts a larger thermal boundary layer than the experiments show. As is apparent, even with a great deal of care with the inlet characterization, it remains very difficult to exactly
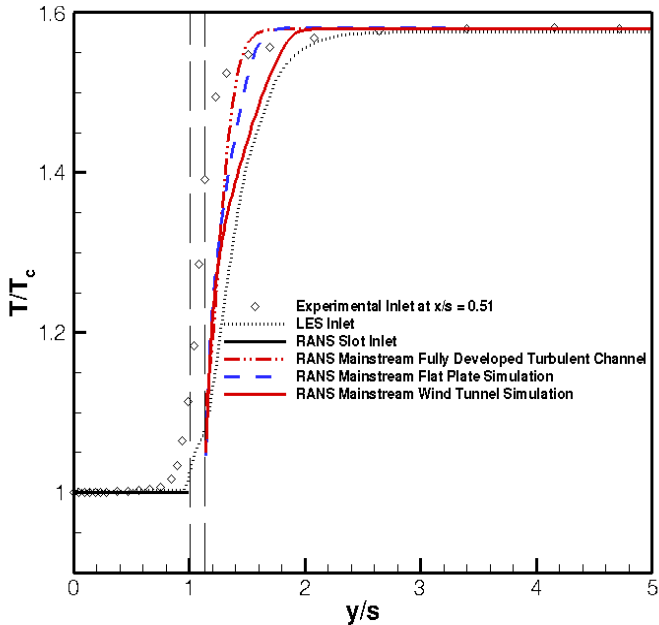

Figure 13. Comparison of wall jet inlet temperature profiles.

48

replicate the experimental inlet conditions. However, it will be shown later that the film cooling results are relatively insensitive to these small differences in boundary layer shape, especially in the mainstream. Even with careful meticulous experimental characterization, a modeler is left with many choices and options for modeling the inflow conditions, the effects of which still needs to be explored.

3.1.2 Film Cooling Results

A wall jet has distinct dynamics that lead to enhanced mixing due to shear. The faster moving coolant tends to spread into the mainstream flow, creating coherent shear vortices with a counterclockwise rotation in the film cooling orientation shown in Figure 4. This large scale turbulent mixing combines with steady state diffusion to further mix the coolant and hot mainstream flows. As it mixes with the mainstream, the coolant gets hotter, thus affording less protection for the wall. For the wall jet, the peak velocity should drop as the mixing layer grows and the flow progresses in the streamwise direction.
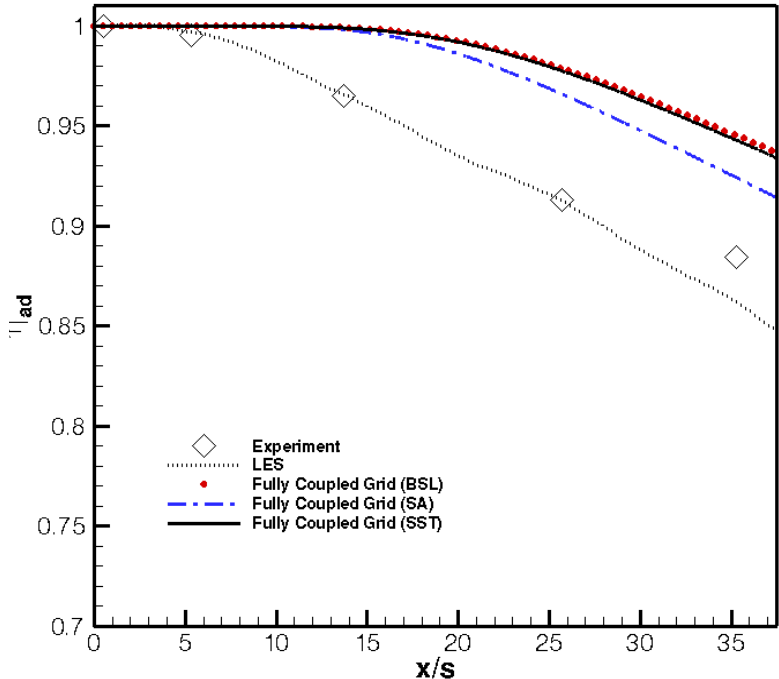
The streamwise evolution of the adiabatic wall effectiveness is shown in Fig. 14 for the SA, BSL and SST models on the fully coupled grid; these simulations are

Figure 14. Comparison of the wall jet film cooling effectiveness.

compared to the experimental data and LES simulation. The relative accuracy of the LES compared to the RANS simulations is a striking feature. The LES simulation captures the effectiveness curve to within 2.5% of the experimental values, while the SA, SST and BSL models are within 4.6%, 6.7% and 7.0%, respectively. The RANS curves have a prolonged, perfect effectiveness region of unity that Simon dubbed the potential core[9]. The potential cores of the RANS curves are all dramatically longer than those of the LES and experiment. Physically, this long effectiveness region of unity means that there is no mainstream fluid, mixed in with the coolant, heating the wall. Of the RANS models, the SA model has the shortest potential core, with the SST and BSL producing nearly identitial results. Roughly speaking, the SA predicts a potential core of 13 slot heights, while the other two RANS models predict potential cores of 15 slot heights. In contrast, the LES simulation faithfully follows the experimental effectiveness, especially in the near-injection field. It has a potential core of roughly four slot heights. The end of this potential core is indicated by the steep change in curvature of the effectiveness curve. Downstream of the potential core, a mixed region of coolant and mainstream fluid create a more rapid decay in the effectiveness. Apart from the length of the potential core and the overall accuracy of a simulation, the effectiveness slope in the far field is also of importance to thermal engine designers, since this dictates the film decay rate. The RANS and LES models seem to overestimate this slope, which for the RANS simulation results in a better prediction of the effectiveness downstream. Meanwhile, the LES effectiveness curve will grow even farther away from the experiment. Further explanation of this phenomenon will be provided later. The RANS and LES simulations also fail to

predict a change in inflection in the adiabatic effectiveness curve. These trends are important for designers as they help determine the downstream decay characteristics.

To better understand the physics of the mixing near the injection region, flow visualization of the original adiabatic wall jet experiment of Cruz[15], taken by Raffan[3], is shown in Fig. 15. The coolant flow is seeded, meaning darker regions in the flow represent mainstream fluid, while brighter regions represent coolant fluid. The mixing between the two streams is unsteady and highly turbulent, even near the inlet, as seen in Fig. 15a. Figure 15c shows the preferred directionality of the coherent, shear structures. This turbulent behavior offers an explanation for the relatively short, initial effectiveness regions predicted by the LES and experimental results. Instantaneous structures infrequently bring a bulk amount of hot, mainstream fluid into the potential core, thus heating the wall more quickly than steady diffusion would predict. RANS models are incapable of picking up this initial, unsteady bulk fluid transport, since all
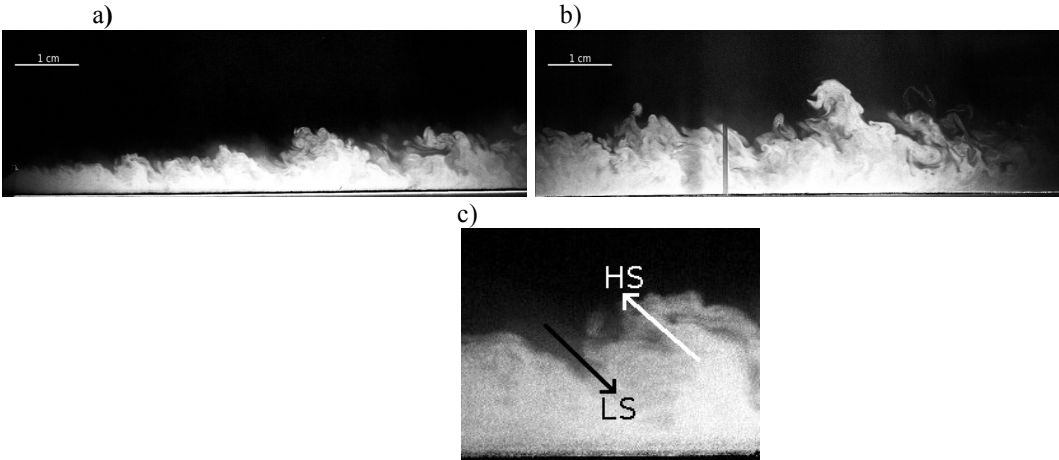
Figure 15. Flow Visualization for Wall Jet case. The initial mixing region, a), and downstream mixing region, b) are shown, along with a close up shot of a coherent structure, c). HS and LS refer to high speed and low speed streaks, respectively. Images reproduced with permission from Raffan[3].

turbulent flow scales are treated uniformly as enhanced diffusion. As the shear layer grows towards the wall, these structures are more likely to bring hot fluid closer to the

wall, resulting in a shorter potential core region than RANS models predict. Also the transition in the wall effectiveness from the potential core to the fully mixed region does not have as sharp of gradients as RANS models predict. At a given time, the turbulent mixing layer instantaneously impinges on the wall at a different streamwise location. This feature would be modeled as the mean mixing layer impinging on the wall at the same location at all times in a RANS simulation. LES picks up this initial region better, since the larger, energy carrying vortices are directly resolved, while the small, dissipative eddies are modeled. Therefore LES simulations have a mechanism
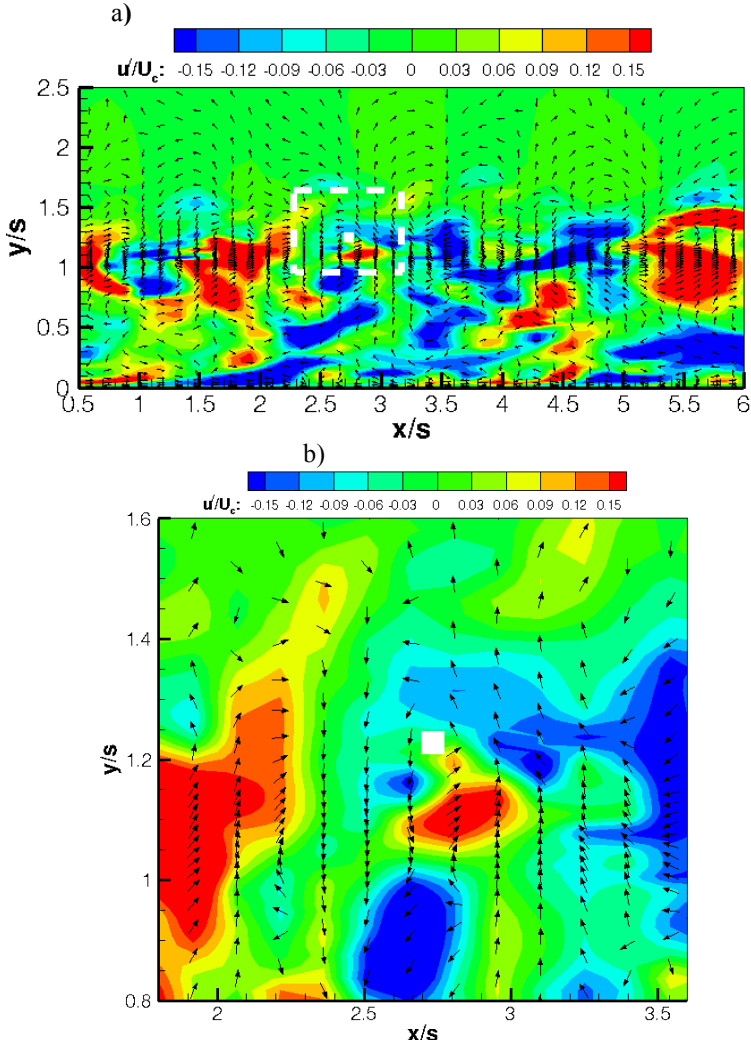
Figure 16. Average normalized u′ contours with instantaneous fluctuating vector field for the LES Wall Jet case. The initial mixing region, a), is shown, along with a close up shot of a coherent structure, b) centered around the white square.

in which bulk mainstream fluid can be carried into the potential core, which is the primary mechanism of effectiveness decay in this region. Figure 16 shows contours of the resolved u' field at an instant in time for the LES simulation. Superimposed on top of that is a vector field based on the instantaneous resolved u' and v' LES field. In Figure 16a, the near injector mixing field is shown, while in Figure 16b a close up of an instantaneous roller structure in the shear layer can be seen. This decomposition of the flow into the streamwise and wall normal fluctuating velocity fields, u' and v', allows for instantaneous shear eddies or roller structures to be easily visualized. The shear structures have a preferred counterclockwise orientation in wall jet flows, which is seen in both Figures 15 and 16. A common misconception is that the long, initial, ideal effectiveness predicted by RANS models is physical. While in high speed flows the initial, near ideal effectiveness is prolonged due to eddies convecting far downstream before impinging on the wall, unsteady, turbulent mixing, in general, tends to increase near wall heating, which reduces the effectiveness in the potential core region. For low speed subsonic film cooling, such as the present experiment and those of Cruz[15] and Raffan[3], the ratio of the convection velocity to the turbulent velocity is much smaller, allowing for large scale turbulent structures to disturb the potential core much closer to injection than for high speed flows.

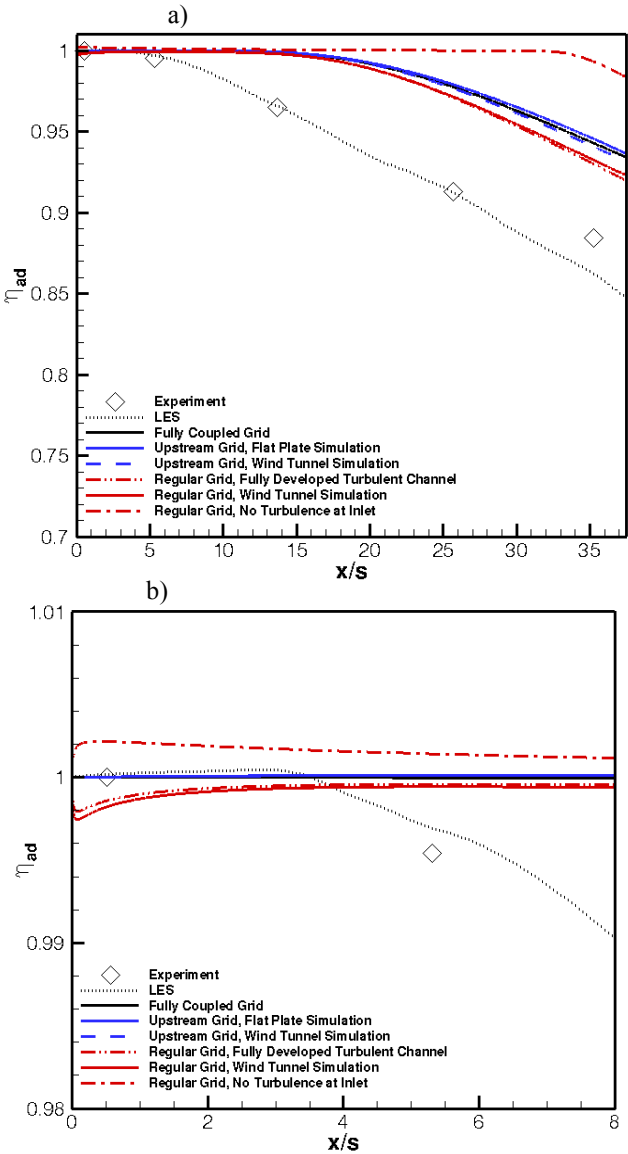One aspect of this canonical film cooling flow that has not been accounted is the formation of the coolant. Recall the coolant is injected into the slot via a small row of holes, before turning and forming a coolant film[15]. This hole injection will tend to create turbulence that is neither isotropic nor symmetric nor fully developed. There will be a relatively higher component of the v' field than a fully developed turbulent

53

channel will indicate. The turbulent Prandtl number is biased towards this v' term due to the fact that there is a v'T' component (the fluctuating vertical velocity multiplied by the fluctuating temperature) in the eddy diffusivity equation that is not in the eddy viscosity equation. Therefore the eddy diffusivity will be increased for this flow, resulting in a smaller turbulent Prandtl number, possibly persisting into the near injector field of the experiment. For RANS models that view turbulence as isotropic, which is the case for the models considered in this study, this constant turbulent Prandtl number assumption might be both too high and inappropriate, especially in the near injector field. Additionally the fully developed turbulent channel assumption will not capture the actual experimental flow field. However, the LES field is introduced in the same way as the RANS field and the LES is still able to resolve the near injector mixing while the RANS cannot. This suggests that the problem is not with the precursor method but rather the resolved flow structures; LES flow structures are able to account for near injector mixing, while the RANS turbulence models do not have this turbulent mechanism.

Figure 17 shows the streamwise progression of the wall jet adiabatic wall effectiveness for a number of different numerical treatments. Effectiveness curves are shown for the LES and experimental results. Figure 17 also shows the RANS adiabatic film cooling effectiveness results of the fully coupled grid, the upstream grid using the mainstream wind tunnel simulation method, the upstream grid using the flat plate simulation, the regular grid using the mainstream fully developed turbulent channel method, the regular grid using the mainstream wind tunnel simulation and the regular grid with no turbulent information specified at the inlet. All the RANS results

presented here have been done with the SST model and use the fully developed turbulent channel method for the slot inflow. The case with no turbulent information prescribed provides the worst estimate of film cooling performance of all the cases studied. This curve has an especially long, potential core that persists even after 30 slot heights in the streamwise direction. By the last station the near injector field is over 12.3% off in terms of adiabatic wall effectiveness, while the error for the cases with turbulence specification range from 5.2% to 7.0%. The poor performance of this case highlights the need for proper turbulent inlet specification; otherwise the near field mixing will be greatly underestimated and film decay will be very inaccurate. The results of the upstream grid and the fully coupled grid using the mainstream wind tunnel precursor simulation are nearly identical, proving that

Figure 17. **Comparison of the film cooling effectiveness for different inlet treatments over a) the entire domain and in b) the near injection region.**

the inflow plane is far enough removed from the injection plane. Therefore almost no error due to decoupling the grid five slot heights upstream of the injection plane exists. The regular grid simulations with turbulent inflow specification behave differently. Even with consistent precursor inlets, as is the case when the wind tunnel simulation is used, the adiabatic effectiveness for the regular grid decays slightly faster, making it seemingly more accurate than the upstream or fully coupled grids. However, the results of this film cooling case show unphysical acceleration near the injection plane causing a rapid change in effectiveness over the first few grid points of the domain, which is not apparent in the upstream and fully coupled grids (see Fig. 17b). This effect is due to the fact that the inlet plane is coincident with the injection plane and fortuitously causes a more rapid decay in the film. Inlet profiles of constant pressure are prescribed exactly on the injection plane, which means the pressure is not allowed to vary. Physically pressure propagates upstream of the injection plane, which is especially apparent when you have a recirculation region existing on the injection plane, in this case at the louver lip. If the pressure is not allowed to vary, according to momentum conservation, the other kinematic properties will adjust and the flow will either accelerate or decelerate in the numerical simulation until the excess momentum is diffused or dissipated. In this case, the flow sharply decelerates over the first few grid points and the wall temperature temporarily increases, resulting in a perceived drop in effectiveness. The effectiveness recovers close to the simulated values of the other cases shortly downstream. The regular grid with no turbulence exhibits a different behavior near the inlet in that the flow accelerates near the inlet causing an increase in effectiveness, suggesting the turbulence affects this inflow specification

56

error. The LES case does not exhibit this unphysical inlet specification because it uses the pressure equation to ensure mass conservation using a low Mach number assumption. Neumann boundary conditions are applied on the pressure field so the inlet pressure will be a function of the kinematic field itself. The film cooling results of the flat plate and fully developed turbulent channel mainstream precursor simulations perform almost identically to those of the mainstream wind tunnel simulation suggesting that the film cooling, especially in the near injection region, is not sensitive to the mainstream mean and turbulent profiles. Therefore, all of the mainstream precursor methods are approximately equivalent for this case as long as the prescribed inflow plane is removed from the injection plane and one of these turbulent methods is used. Therefore, in the rest of this paper the wind tunnel simulation is selected as the precursor simulation because of its ease of use and the other benefits listed in Chapter 2. Additionally, URANS results showed no noticeable differences from the steady results, suggesting that for this louver lip thickness to slot height ratio of 0.14 no large scale periodic wake shedding is present.

The flow effectiveness provides a measure of the amount of thermal mixing at a given spatial location and is defined as

$$\eta_{flow} = \left(T_\infty - T\right)\big/\left(T_\infty - T_c\right) \tag{11}$$

where T_∞, T_c and T are the mainstream, coolant, and local flow temperatures, respectively. The effectiveness is a non-dimensional temperature that gives an insight into local mixing, allowing features such as the shear layer to be visualized in terms of the thermal field. Figure 18 shows the flow effectiveness contours for the RANS fully coupled grid simulation and the regular grid with no prescribed turbulence simulation.

Also the LES mean resolved flow effectiveness contours are shown in Figure 18. The effectiveness in these plots have contours truncated at 0.8 so the near wall mixing can be more easily seen. The actual range of contours does go down to zero in the mainstream, but any effectiveness values lower than 0.8 were aliased to the 0.8 contour. Each contour level represents a 0.01 change in flow effectiveness. Using Figs.
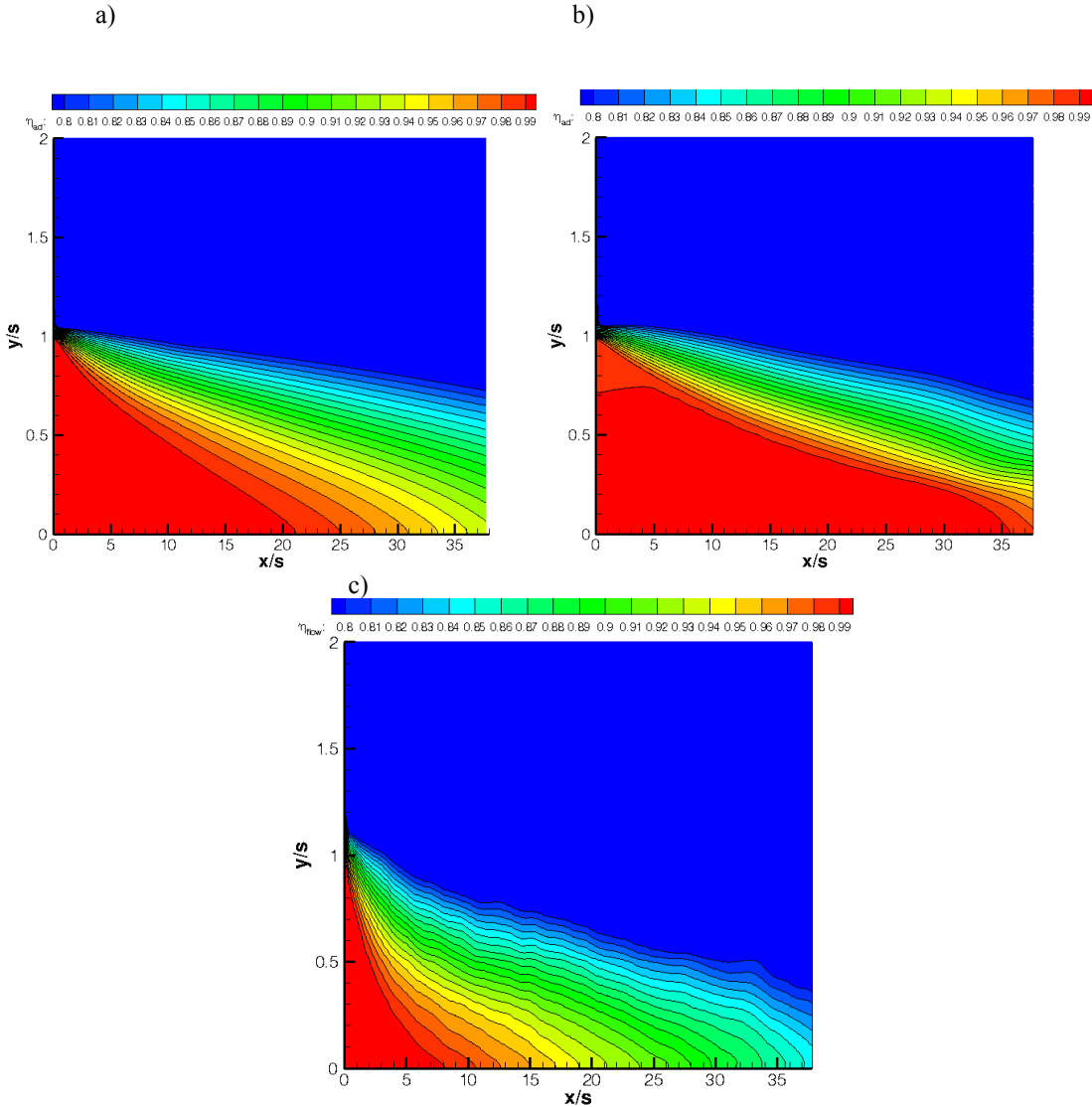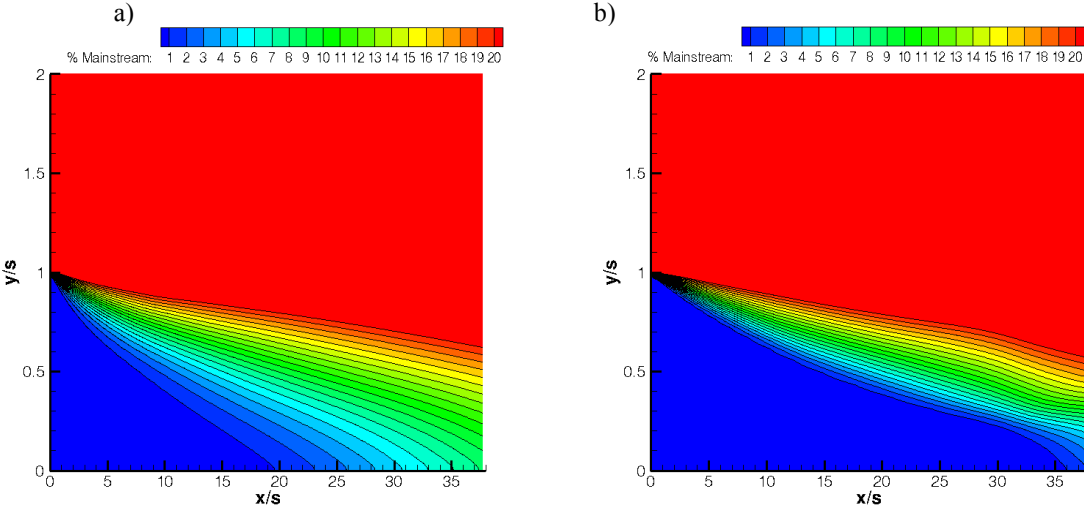

Figure 18. **Comparison of the wall jet flow effectiveness contours for a) the fully coupled film cooling simulation, b) the regular film cooling simulation with no prescribed turbulence and c) the LES film cooling simulation.**

17 and 18, the end of the potential core, or the streamwise location where the mean mixing layer impinges on the wall, occurs at x/s of 21, 36 and 8 for the fully coupled grid, the regular grid with no turbulence and the LES simulation, respectively. Here the end of the potential core is defined as the place where adiabatic wall effectiveness is 99% of its original value. At these points in the curves in Fig. 17, the effectiveness rapidly changes slope and eventually approach a relatively steady slope, as is evidenced by the consistent spacing of the effectiveness contours at the wall in Fig. 18. The LES contour is dramatically different than the other two RANS contours. The impingement point of the thermal mixing layer on the wall occurs much sooner for the LES case than either of the RANS simulations. Secondly the mean spread rate is much faster and the edge of the mixing layer is more nonlinear than for the RANS curves, further highlighting the differences in mixing between the two flows.

Figure 19 shows contours of the mainstream mass fraction for the two RANS cases just mentioned. The contours were truncated at 20% mainstream fluid for visualization purposes. These plots physically show the lower extent of the mixing layer, which line up well with the effectiveness contours. From these results, the mixing layer impinges on the wall 20 and 36 slot heights downstream of injection for the two cases, respectively. The mixing layer growth rate occurs much faster for the fully coupled results than for the case with no prescribed turbulence, showing the mixing enhancement due to turbulence at the inlet. There is some variability between the mass and thermal results, since what constitutes impingement is somewhat vague; for these results, the first mixing layer contour line that hit the wall defined the end of the potential core. Alternatively the potential core is defined by the 99 % point based on

coolant mass. The similarity in these two sets of contours show for RANS simulations that the mechanisms governing mixing are analogous between the thermal and mass fields. These findings confirm the hypotheses of Simon[9] that the potential core is the near ideal effectiveness region, where the mixing layer has not yet reached the wall, and the mixing layer impinging on the wall results in a rapid change in effectiveness, thus changing the film decay rate.

Figure 19. **Contours of percent mainstream mass for a) the fully coupled film cooling simulation and b) the regular film cooling simulation with no prescribed turbulence .**

Streamwise mean velocity profiles at the inlet and at different downstream streamwise axial stations are shown in Fig. 20. As is expected, there are steep gradients in the first profile at the wall and in the shear layer. The experimental data has data dropout near the wall due to noise in the PIV measurement. The data has once again been truncated to include only physically meaningful data. The upper extent of the shear layer is visualized by the inflection change in curvature that occurs at the furthest point away from the wall. The streamwise progression of profiles show that the gradients in the shear layer both decay and spread as the higher momentum coolant

60

flow diffuses, in a mean sense, into the mainstream. Between the inlet and the first measurement station, none of the profiles are significantly different than their inlet values. By the first downstream measurement, all the profiles have started mixing with the LES overpredicting the shear layer growth rate in this region. It should be noted that the experimental inlet is actually experimental data taken 0.37 slot heights downstream of injection. By 5.3 slot heights downstream of injection, all the numerical curves slightly underestimate the extent of the shear layer, with the LES curve providing the closest estimate. Closer to the wall, the LES curve begins to lag
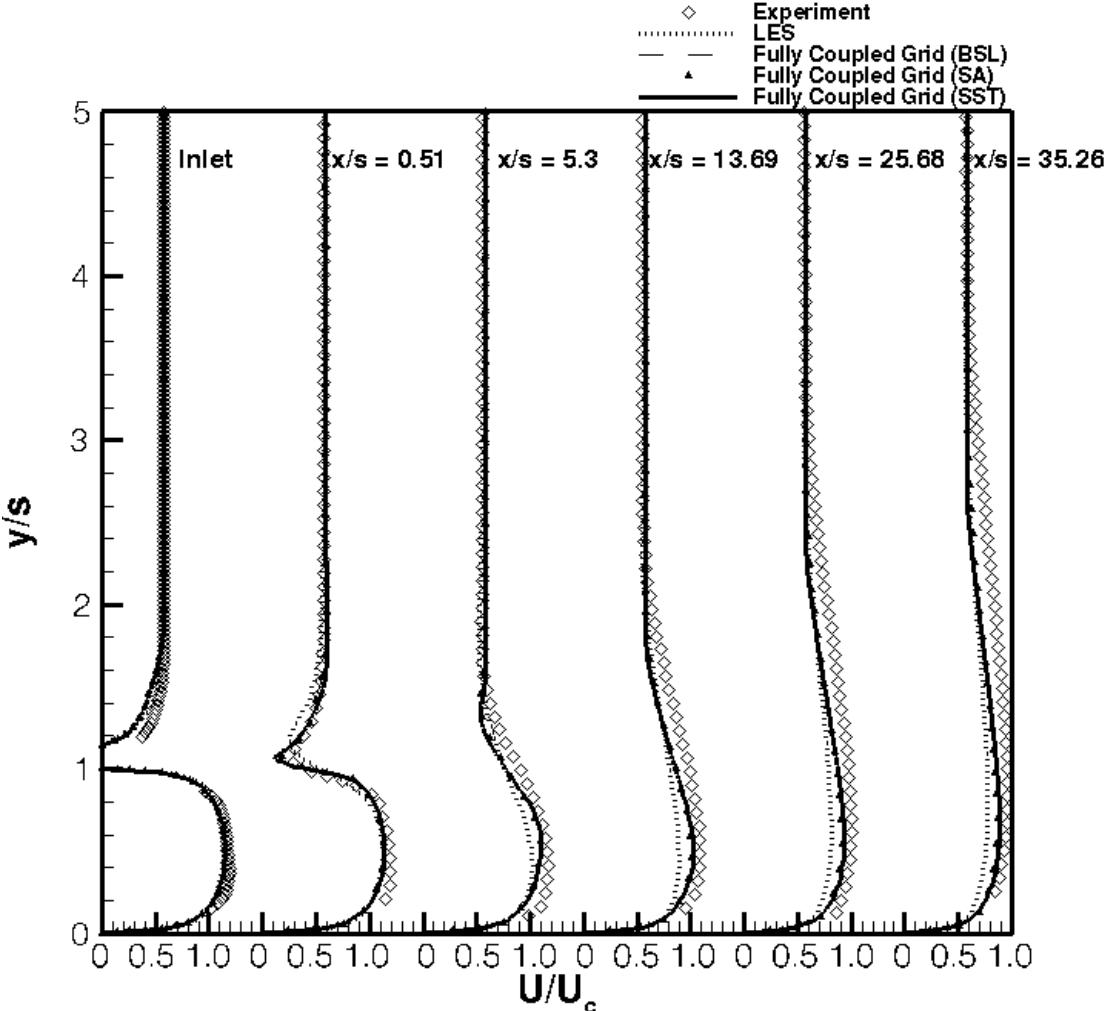

Figure 20. Comparison of velocity contours at different streamwise locations.

behind the other computational and experimental profiles. As the profiles develop in the streamwise direction, the LES curve lags more behind the other profiles, while the extent of the shear layer remains underpredicted by the computational curves with all numerical simulations performing approximately the same. By the end of the film cooling domain, the velocity profiles begin to resemble a boundary layer, whose gradients and flow evolution should be accurately resolved by most RANS solvers. In general, the velocity field is resolved better by the RANS solution. The RANS results slightly underpredict the peak velocity, while the LES results show a more appreciable deficit in the velocity profile downstream, highlighting the constant density assumption in the code. For a given momentum, the LES predicts a higher density and therefore a lower velocity, since the code is non-dimensionalized based off of the slot quantities. Therefore as the coolant is heated, thermal effects cause the coolant to accelerate. The shear and diffusion of momentum conversely cause the coolant to decelerate in this wall jet case. The LES simulation cannot resolve the thermal acceleration properly causing the LES velocity curves to lag behind the other variable density curves. There are other effects such as non-constant viscosity and thermal conductivity that would influence these trends as well, but were ignored for this simple analysis. The initial shear layer growth rate, as is indicated by the inflection change of the velocity curve, seems to be better estimated by the LES results than the RANS simulations. The RANS and LES velocities are both captured to within 19.1% of the experimental data, respectively. Overall, the mean streamwise velocity trends are captured well by the RANS simulation due to the variable density effects just discussed.

These momentum results also provide some insight into the constant density LES mixing trends, especially in terms of the streamwise progression of adiabatic wall effectiveness. The LES energy equation is shown in Eq. 12 below.

$$\frac{\partial \overline{T}}{\partial t} + \frac{\partial \overline{T}\overline{u}_j}{\partial x_j} = \frac{1}{\text{Re}\,\text{Pr}}\frac{\partial^2 \overline{T}}{\partial x_j \partial x_j} - \frac{\partial q_j}{\partial x_j}$$

(12)

This equation uses Einstein notation, with the overbar denoting spatial filtering. Re, Pr and q represent the Reynolds number, the Prandtl number and the subgrid scale heat flux, respectively. If the transients, axial, and spanwise diffusion and spanwise convection are neglected, along with the subgrid scale heat flux, this equation can be simplistically recast as Eq. 13.

$$\frac{\partial \overline{T}\overline{u}}{\partial x} = \overline{u}\frac{\partial \overline{T}}{\partial x} + \overline{T}\frac{\partial \overline{u}}{\partial x} = -\frac{\partial}{\partial y}\left(\dot{q}_y''\right) \text{ with } \dot{q}_y'' = \overline{T}\overline{v} - \frac{1}{\text{Re}\,\text{Pr}}\frac{\partial \overline{T}}{\partial y}$$

(13)

The heat flux $\dot{q}_y''$ is defined as positive away from the wall. In the wall jet film cooling case, as the flow progresses downstream, a heat flux is generated towards the wall meaning the convection term in the x, or streamwise, direction will be a positive value. If we further assume, the velocity changes slowly in the streamwise direction in comparison with the thermal gradient, it can be shown that the temperature gradient behaves as is shown in Eq. 14.

$$\frac{\partial \overline{T}}{\partial x} = -\frac{1}{\overline{\overline{u}}}\frac{\partial}{\partial y}\left(\dot{q}_y''\right)$$

(14)

As the kinematic results show, the LES constant density velocity lags behind the variable density velocity of both the RANS and experimental results near the wall in the far field. Eq. 14 shows that the temperature decay is inversely proportional to the streamwise velocity gradient. Therefore with a lower velocity, the streamwise gradient

in temperature will be a larger positive number, meaning that the constant density temperature in the film will increase more rapidly than it would in a variable density calculation. A variable density LES, therefore, should provide even better mixing performance than the constant density case because the overprediction in the streamwise temperature gradient in the far field should be better resolved.

Figure 21 shows the resolved turbulent kinetic energy versus wall normal distance at the inlet and several downstream distances for the experiment, the LES simulation and the fully coupled grid RANS results using the BSL and SST turbulence models. The experimental data at the inlet was derived from turbulent kinematic information prescribed at 0.37 slot heights downstream of the injection plane, meaning the slot turbulent kinetic energy profiles have already started expanding and interacting with the mainstream boundary layer. The data is truncated to the first valid data point, which occurs near the peak in the turbulent kinetic energy. As the two streams meet, the turbulent kinetic energy dramatically increases in a very narrow mixing region. As the flow progresses, this peak decreases and spreads, eventually assuming a boundary layer like shape far downstream. Even at the last measurement station there is still evidence of this mixing region resulting in a shape differing from that of a boundary layer. The RANS simulations underestimate the turbulent kinetic energy in the near injector field. However as the flow progresses downstream and assumes a boundary layer shape, the RANS simulation start better capturing the turbulent kinetic energy trends relative to the experiment. The LES conversely overpredicts the peak turbulent kinetic energy relative to the experiments by as much as 63% especially in the mixing layer at the first downstream measurement location where the shear is the highest, but

also underpredicts the experiment in rest of the slot region. As the flow moves past 13.69 slot heights downstream, the LES profiles begin to underestimate the turbulent kinetic energy but are very close to the experiment. Overall the RANS simulations dramatically underpredict the turbulent kinetic energy by as much as 38% of the experimental values, leading to reduced mixing and therefore higher adiabatic wall effectiveness.
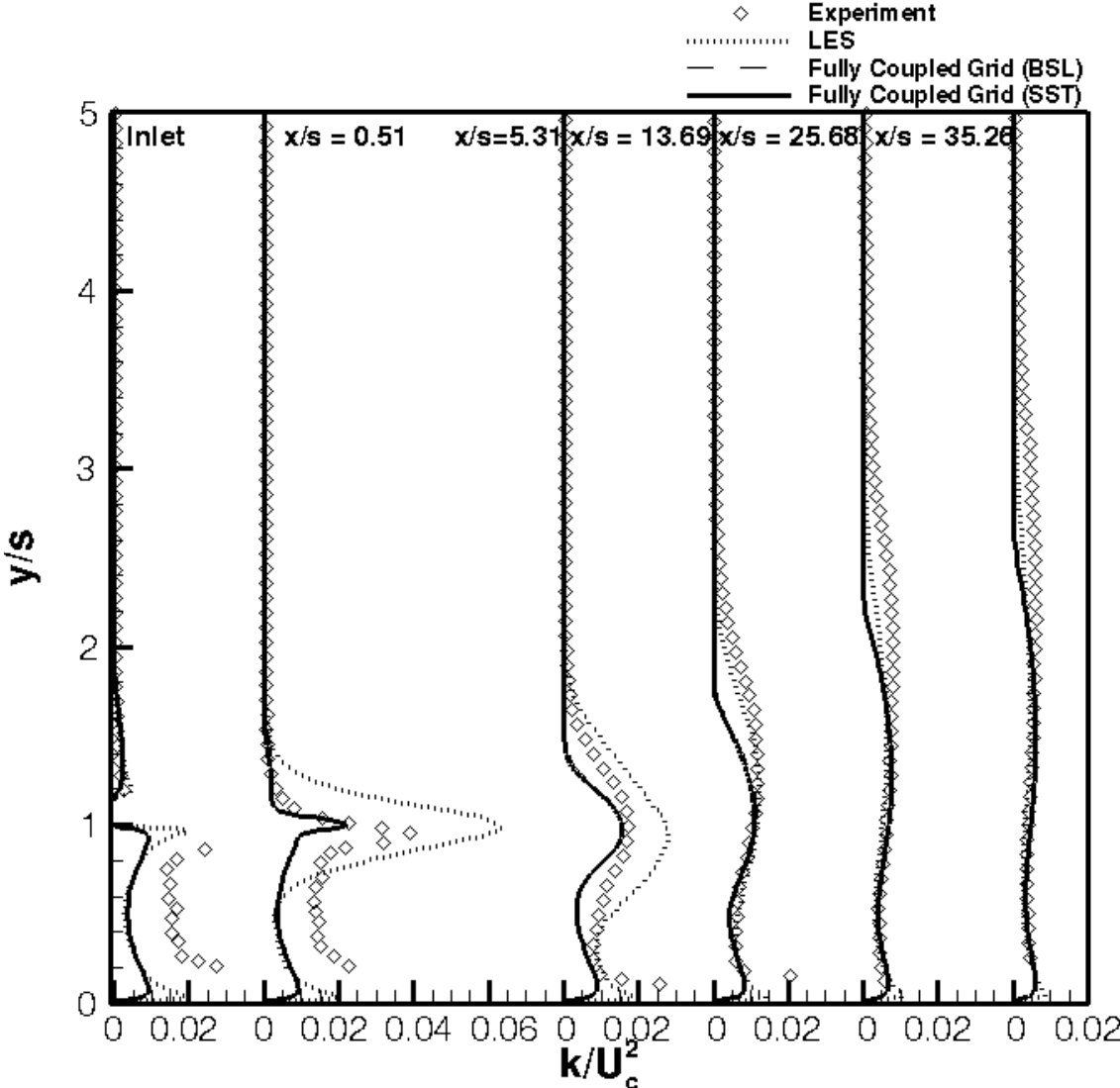

Figure 21. Comparison of turbulent kinetic energy contours at different streamwise locations.

Temperature profiles non-dimensionalized by the bulk coolant temperature are shown in Fig. 22 at several different downstream locations along with the inlet for the experiment, LES and the fully coupled grid for all the turbulence models. Similarly Fig. 23 shows the flow effectiveness contours at the inlet and several downstream locations, providing a direct measure of thermal mixing. There is no experimental thermal profile at the inlet, since the first downstream thermal profile is also the first streamwise profile that is available and is used to characterize the thermal inlets. The
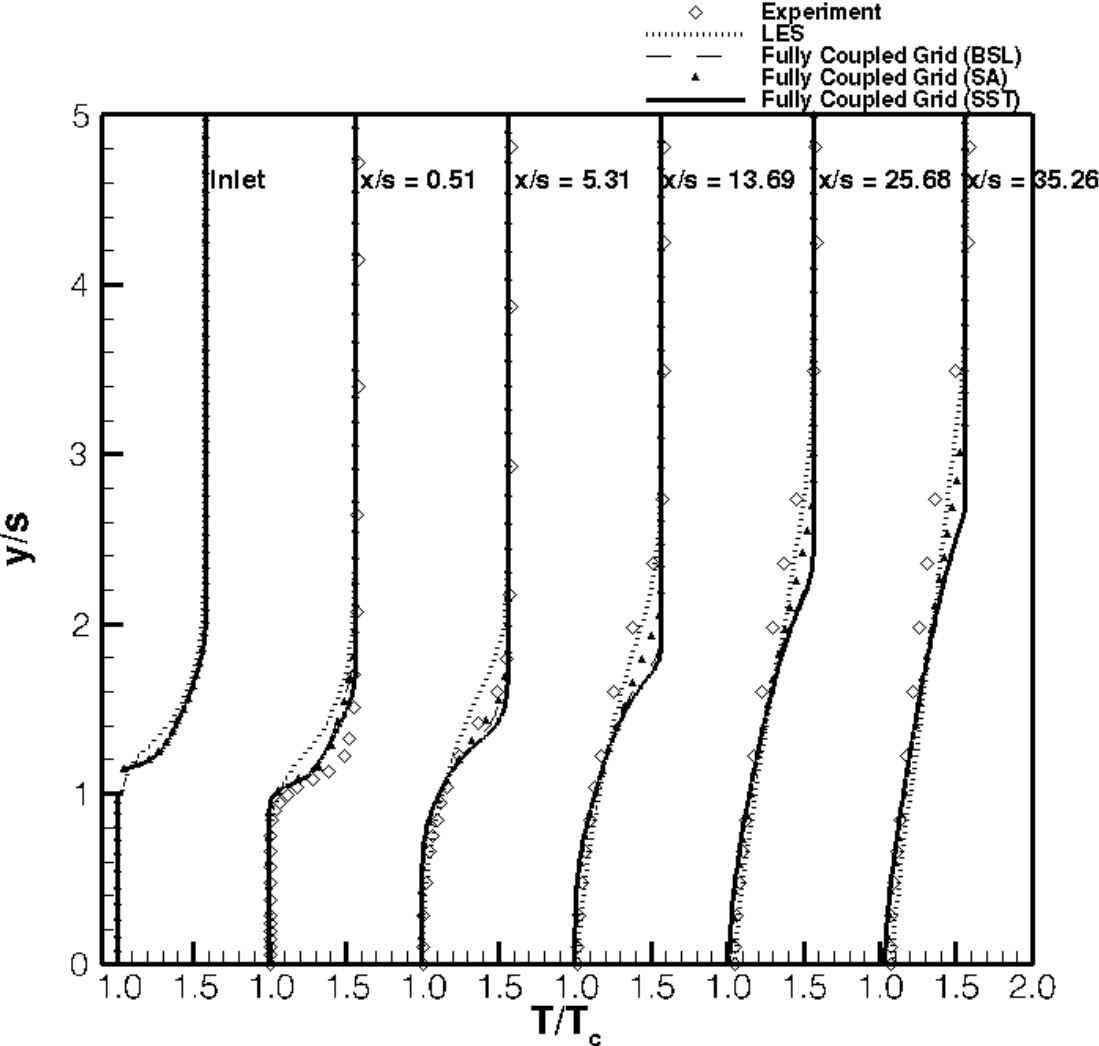

Figure 22. Comparison of temperature contours at different streamwise locations.

thermal mixing layer growth rate, especially in the near field, is underpredicted by all the RANS simulations, which translates to reduced mixing of the coolant. As is seen in the turbulent kinetic energy, the LES results overpredict the growth rate of the mixing layer in the near field but begin to start underpredicting the growth rate near the third downstream measurement location. Interestingly, the RANS results also depict a sharper gradient at the edge of the mixing layer. The LES and experimental fields do not seem to show these sharp gradients at the extent of the mixing layer, which seems
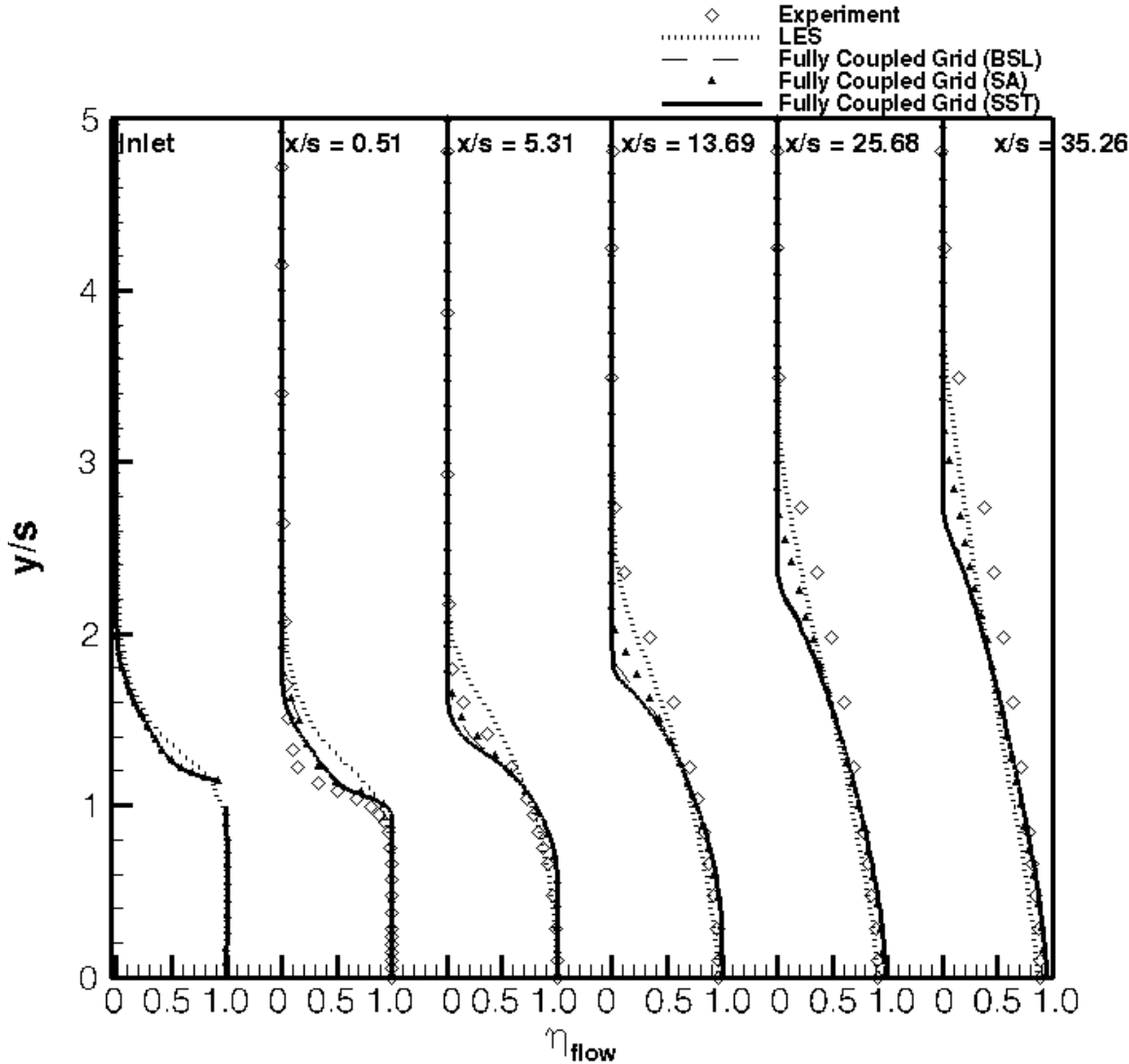

Figure 23. Comparison of flow effectiveness contours at different streamwise locations.

to be more physical, since these gradients should gradually end as occurs in both molecular and turbulent diffusion processes. RANS models have no mechanism for intermittent mixing at the edges of the mixing layer causing a sharper end to the mixing region than LES and experimental fields would predict. As the gradients diffuse and the coolant jet expands, the RANS flow temperatures remain underpredicted, especially at the last two streamwise stations. The Spalart-Allmaras captures the temperature progression better than the other two RANS models, with the LES performing the best of all the simulations, especially in terms of thermal mixing as is shown in the effectiveness results shown in Figures 14 and 17. In fact the LES captures the temperature to within 5.0 % of the experimental values in the far field, whereas the BSL, SA and SST are within 13.1 %, 10.4 % and 13.2 %, respectively.

The LES dynamically solves independently for both the turbulent eddy viscosity and diffusivity, leading to a variable turbulent Prandtl number. These findings seem to suggest either that the constant RANS turbulent Prandtl number of 0.7 could be too high since more turbulent thermal diffusion is necessary in the near field, or that the constant turbulent Prandtl number assumption could be less valid in different regions of the flow, namely in regions of large shear or near a separation region.

3.2 Minimum Shear Film Cooling Case

The minimum shear film cooling scenario features two streams that carry approximately the same momentum, resulting in lower shear and therefore lower mixing. Distinctly different from either the wall jet or wall wake scenarios, the minimum mixing layer features roller structures with no preferred direction of rotation. Similarly, the coolant and mainstream diffuse into each other equally

68

resulting in an unslanted mixing layer. For example, in the wall jet scenario the mixing layer is slanted towards the mainstream, since in a mean sense momentum diffuses into the mainstream. Theoretically a minimum shear scenario affords the most efficient film cooling, since it results in the least amount of mixing per unit mass of coolant.

3.2.1 Film Cooling Results

Figure 24 shows the adiabatic wall effectiveness for the corrected experimental data and the fully coupled grid RANS simulations using the BSL, SA and SST turbulence models. Once again the SA performs the best of the RANS models, predicting the performance to within 4.8% of the experiment. The SST and BSL meanwhile capture the film effectiveness to within 6.4% and 6.6 %, respectively. All the RANS results show a significantly longer potential core than the experimental results, with the SA, SST and BSL models nominally predicting the point of mean mixing layer impingement occurring at 11, 15 and 15 slot heights downstream of injection, respectively. The experimental data also seems to show an inflection point in the experimental data, which is not captured by the RANS data.
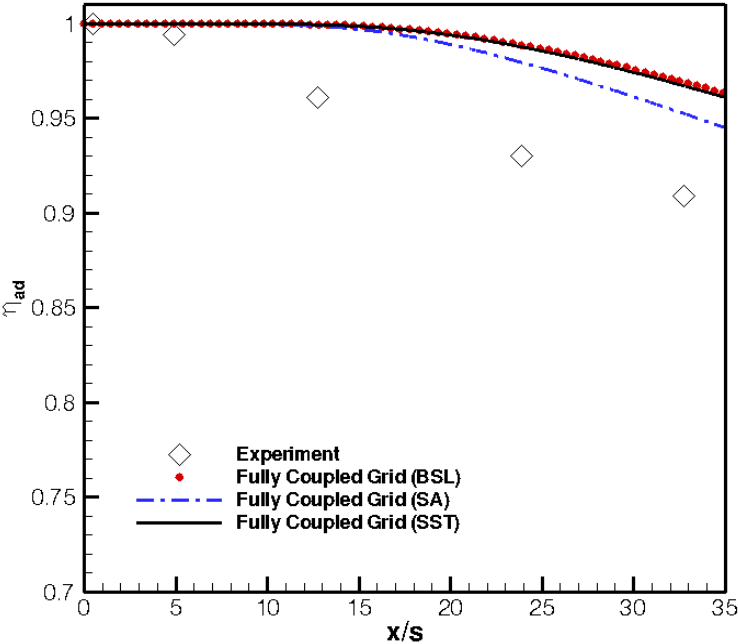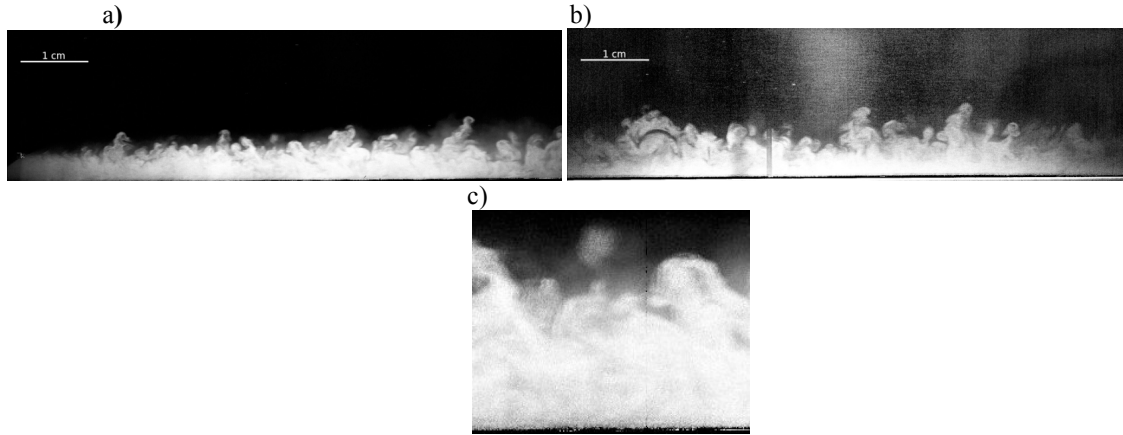
To better understand the

Figure 24. Comparison of the film cooling effectiveness for the minimum shear case.

69

Figure 25. **Flow Visualization for the Minimum Shear case. The initial mixing region, a), and downstream mixing region, b) are shown, along with a close up shot of a typical shear structure, c). Images reproduced with permission from Raffan[3].**

kinematics of the minimum shear case, flow visualization from the adiabatic minimum shear film cooling experiment of Raffan[3] are reproduced below in Figure 25. Once again we can see, several different roller structures, but on average they have no preferential orientation. Also the mixing layer remains thinner than the wall jet case since the mixing layer spread is governed by molecular and turbulent diffusion only, without the added advection component apparent in the wall jet case. Also between the two flow visualizations the film seems to remain stronger near the wall than the wall jet. The side edges of the flow visualization are dimmed due to limited beam width of the shadowgraph laser.

Mean streamwise velocity profiles are shown at the inlet and several downstream locations for the experiment and RANS simulations in Figure 26. The experimental inlet was actually derived from data 0.35 slot heights downstream of injection. All the RANS models perform nominally the same, with the velocity results being predicted to within 10.9 % by all RANS simulations after the first downstream measurement

location. The shear layer growth rate is slightly underpredicted, but in general the RANS follows the experimental curves very faithfully. Once again the gradients at the extent of the mixing layer seem unphysically sharp, but overall the RANS results pick up the mean kinematic features of the minimum shear film cooling case. The mixing layer growth is reduced for this minimum shear case with respect to the wall jet scenario.

Figure 27 shows the turbulent kinetic energy of the experiment and the BSL, and SST RANS fully coupled grid calculations. Once again the RANS results underpredict
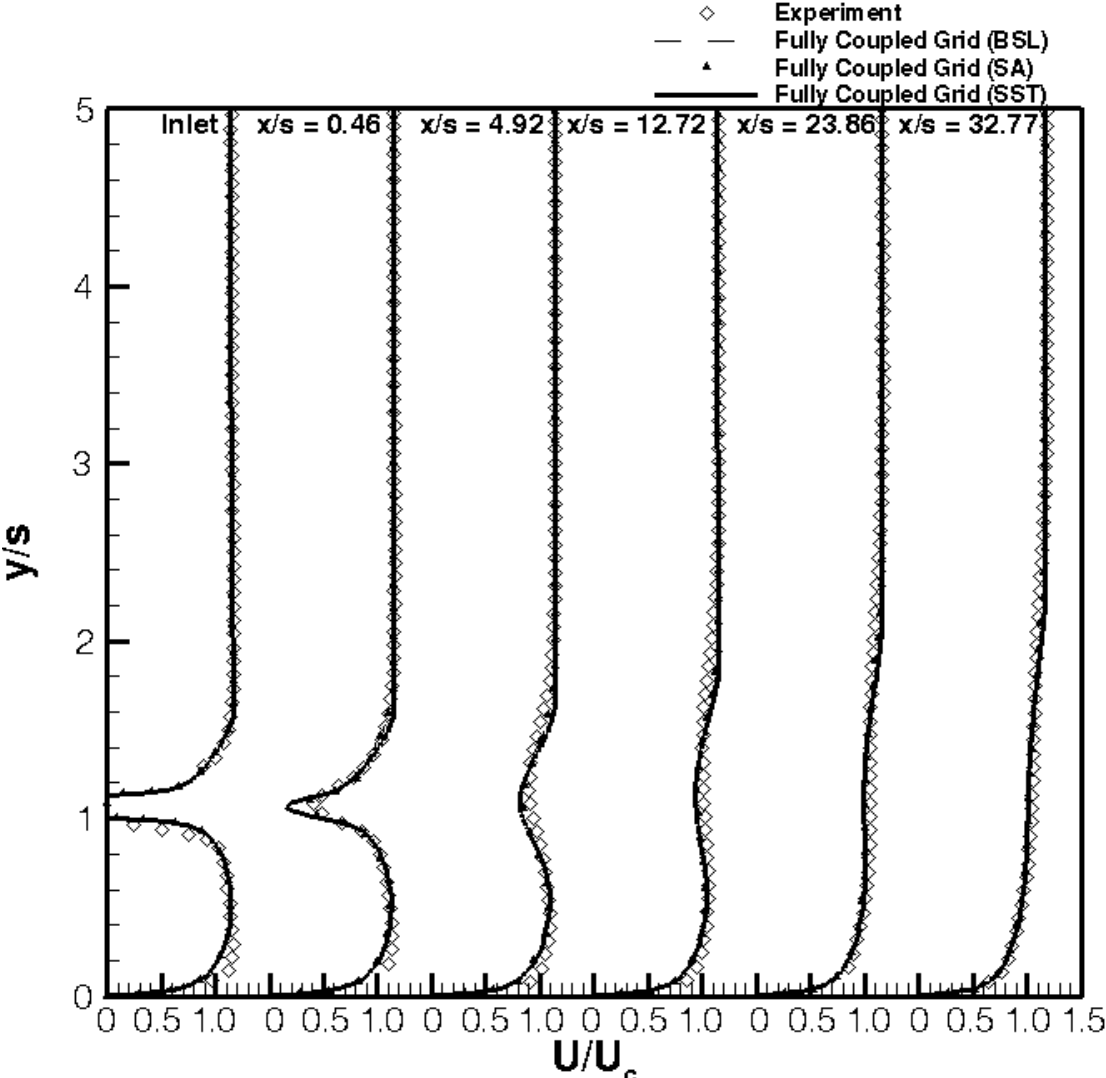

Figure 26. Comparison of streamwise velocity contours for the minimum shear film cooling case.

the turbulence levels throughout the flow but most dramatically in the near injector region, with the peaks being 20 % of the experimental values. Even though the initial turbulent kinetic energy peak in the mixing layer is underpredicted, the numerical results downstream agree very well with the experiment, with just the mixing layer growth being underpredicted. At 0.46 slot heights downstream of injection, the turbulent kinetic energy peaks from the slot and mainstream flows have not combined in the RANS simulations, which is not the case for the experiment. This reduction in the turbulent kinetic energy is most likely a major cause of the initial underprediction
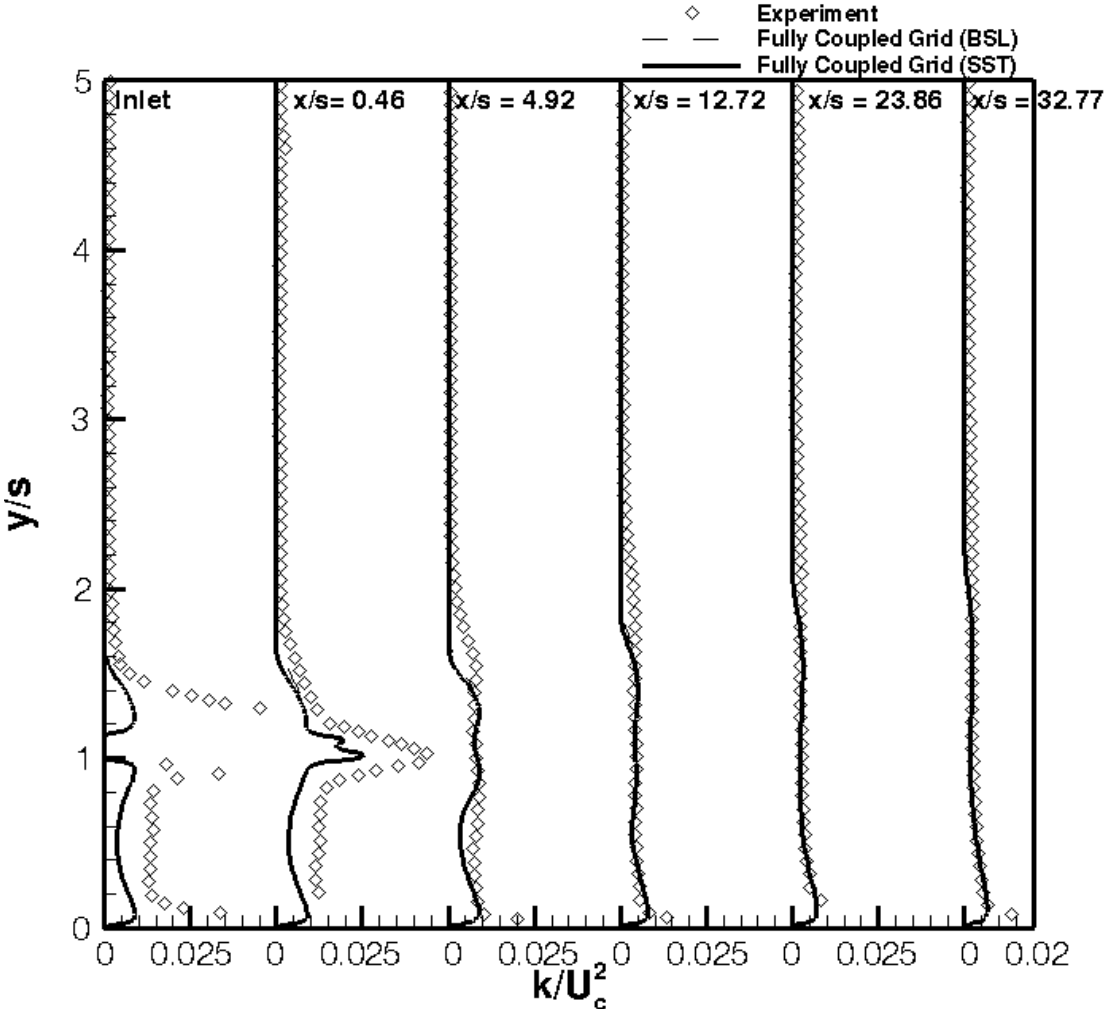

Figure 27. Comparison of streamwise turbulent kinetic energy contours for the minimum shear film cooling case.

of film decay. By the second downstream measurement station, however, the peaks in the turbulent kinetic energy are well predicted by the RANS simulations.

Figures 28 and 29 show temperature contours and flow effectiveness contours, respectively, for the minimum shear experiment and RANS simulations at several different downstream stations. Once again no experimental inlet is shown, since the first downstream thermal measurement is the closest measurement to the injection plane available. The data missing in the inlet profile corresponds to temperature measurements through the louver. In terms of the wall temperature, the RANS
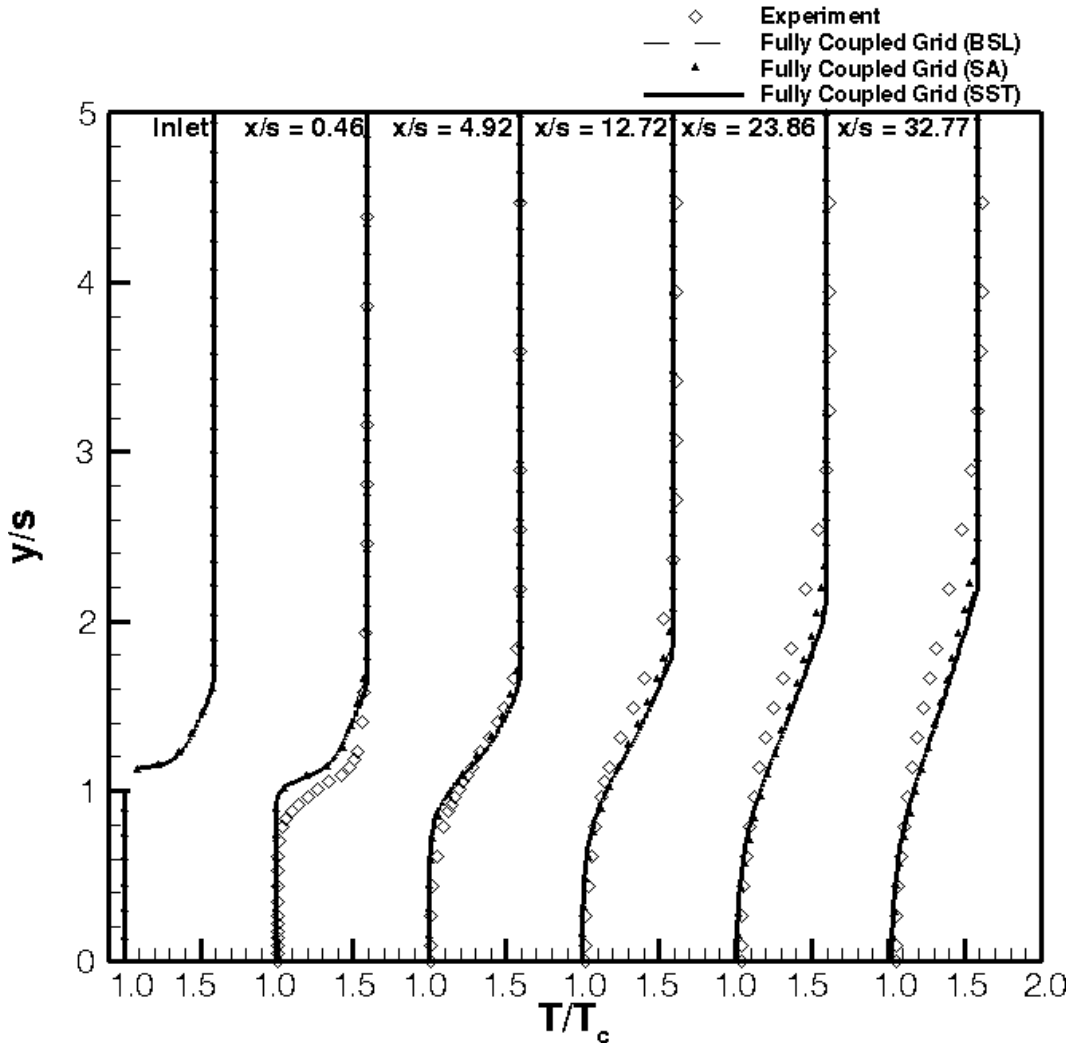

Figure 28. Comparison of temperature contours for the minimum shear film cooling case.

simulations lag behind the experiment resulting in a lower wall temperature and a correspondingly, higher film effectiveness. Thermally the mixing layer spreads less than the wall jet scenario. Even for this shear case, the thermal mixing is underpredicted by the RANS simulations, with the SA model predicting the most spreading of the three models. Overall the near wall mixing is captured well, while away from the wall in the far field the agreement starts to differ as the mixing layer spread rate is not accurately captured. While initially, the thermal field is prescribed incorrectly, by the second downstream measurement location most of the experimental thermal field is accurately resolved by the RANS simulations. In fact in the far field, the temperature is calculated to within 12.3 %, 9.7 % and 11.1 % of the experimental values by the BSL, SA and SST turbulence models, respectively.

3.3 Wall Wake Film Cooling Case

The wall wake experiments are also simulated. The dynamics of a wall wake are distinctly different than those of a wall jet. In this scenario, the coolant is the slower moving fluid, allowing the mainstream to spread in a mean sense towards the wall. The coherent roller structures have the opposite sign of the wall jet. Due to their orientation, the structures should correspondingly entrain hot fluid towards the wall more quickly than the wall jet. Not surprisingly, the decay in effectiveness is initially more rapid. The velocity profiles resemble a wake flow. As the flow progresses in the streamwise direction, the velocity deficit near the wall decreases and the flow eventually resembles a boundary layer.
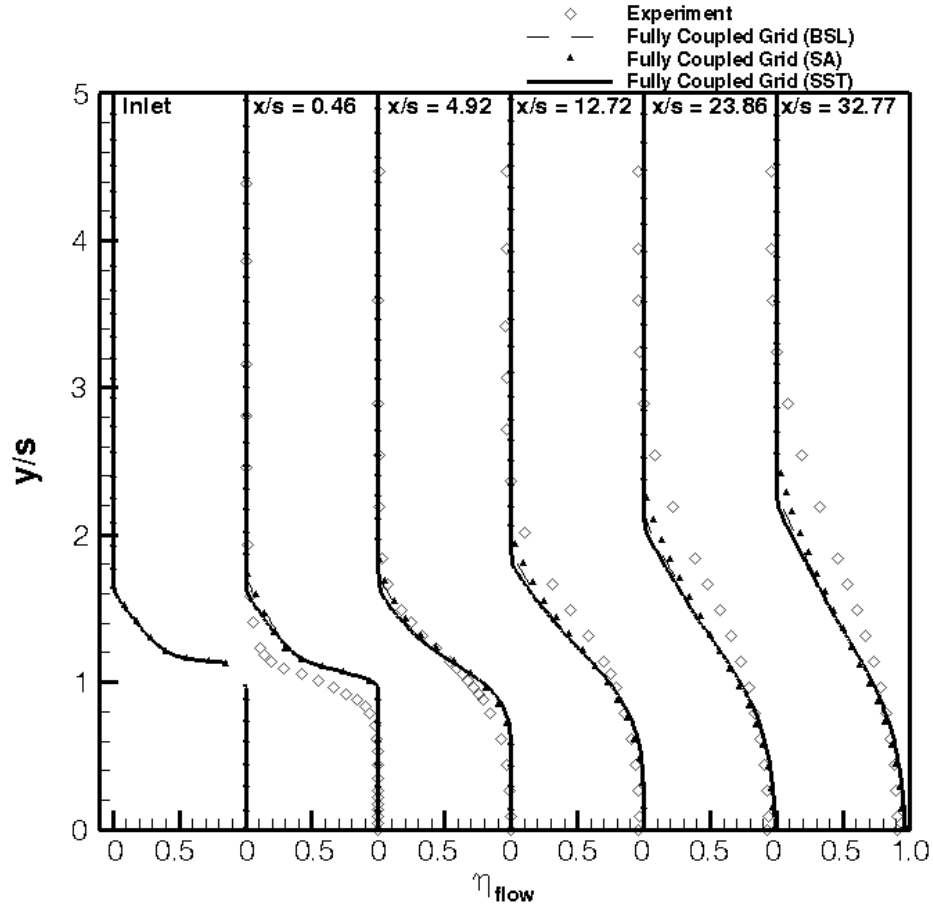
Figure 29. Comparison of flow effectiveness contours for the minimum shear film cooling case.

3.3.1 Film Cooling Results

Figure 30 shows the streamwise progression of the adiabatic wall effectiveness for the experiment and the fully coupled grid simulations using the SST, BSL and SA models. The SST, BSL and SA models capture the experimental
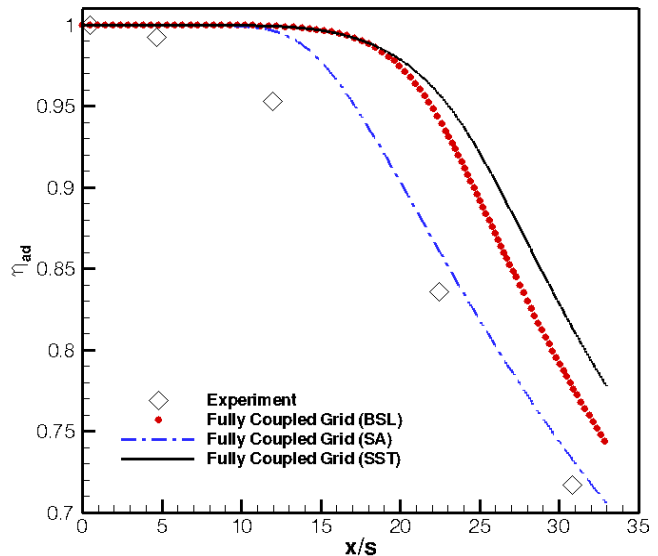

Figure 30. Comparison of the film cooling effectiveness for the wall wake.

effectiveness within 13%, 11% and 4.6% respectively. Notice the initial rapid decay of the experimental effectiveness profile, leading to a much shorter potential core region than for the wall jet case. The RANS results dramatically, overpredict this potential core, with the SA model once again providing the most accurate streamwise progression of adiabatic effectiveness. It should be stated that the temperature in the near wall region, especially in near injector field, is susceptible to contamination via radiation effects. The first few measurement points have been corrected to account for this radiation error. For the experimental profile the minimum temperature was taken as the wall temperature, since the apparent wall temperature was a few degrees hotter than the minimum temperature due to this radiation effect. Since there is no mechanism for the wall to be hotter on average than the flow, this was deemed to be valid. After the potential core ends, the film cooling effectiveness experiences a sudden, rapid decay. As the mixing layer reaches the wall and the flow resembles a boundary layer, the film decay rate seems to be better captured, which is not surprising, since boundary layers are often benchmark studies for RANS models. All numerical results seem to indicate a downstream inflection change, which is not apparent in the experimental data but is present in correlation models[13]. Also somewhat surprising, is that the BSL starts to differ from the SST in this case. The SST and BSL turbulence models are only slightly different, with the SST incorporating the transport of the principle turbulent shear stress into the eddy viscosity, which is intended to help in the wake region of flows where adverse pressure gradients are present[21]. This further highlights that turbulence models behave differently depending on the shear scenario making the accurate simulations of film

76

cooling flows difficult. Flow visualization of the wall wake case performed by Raffan[3] is shown in Figure 31. Here the typical clockwise roller structures associated with wall wakes can be seen. Since the roller structures rotate towards the wall, the length of the potential core is dramatically reduced as discussed previously. This mixing mechanism results in the shortest potential core in any of the cases, leading to the largest overprediction of mixing layer the impingement length.
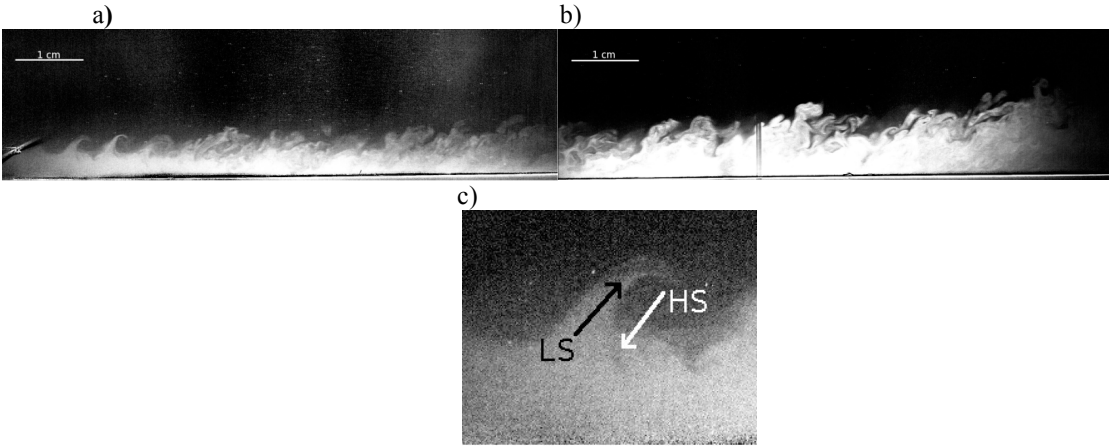
Figure 31. **Flow Visualization for the Wall Wake case. The initial mixing region, a), and downstream mixing region, b) are shown, along with a close up shot of a coherent structure, c). HS and LS refer to high speed and low speed streaks, respectively. Images reproduced with permission from Raffan[3].**

The mean streamwise wall wake velocity profiles can be seen in Figure 32 for the experiment and the three RANS simulations. The kinematic inlet is characterized 0.42 slot heights downstream of injection. Here the initial velocities in the slot are slightly overestimated by the numerical simulation as opposed to the underprediction in the previous two cases. The velocity is once again matched extremely well between the experiment and the simulations, with the spread rate being underpredicted relative to the experimental results. Once again, very sharp gradients occur at the extent of the mixing layer, which is not apparent in experimental results. In this scenario the
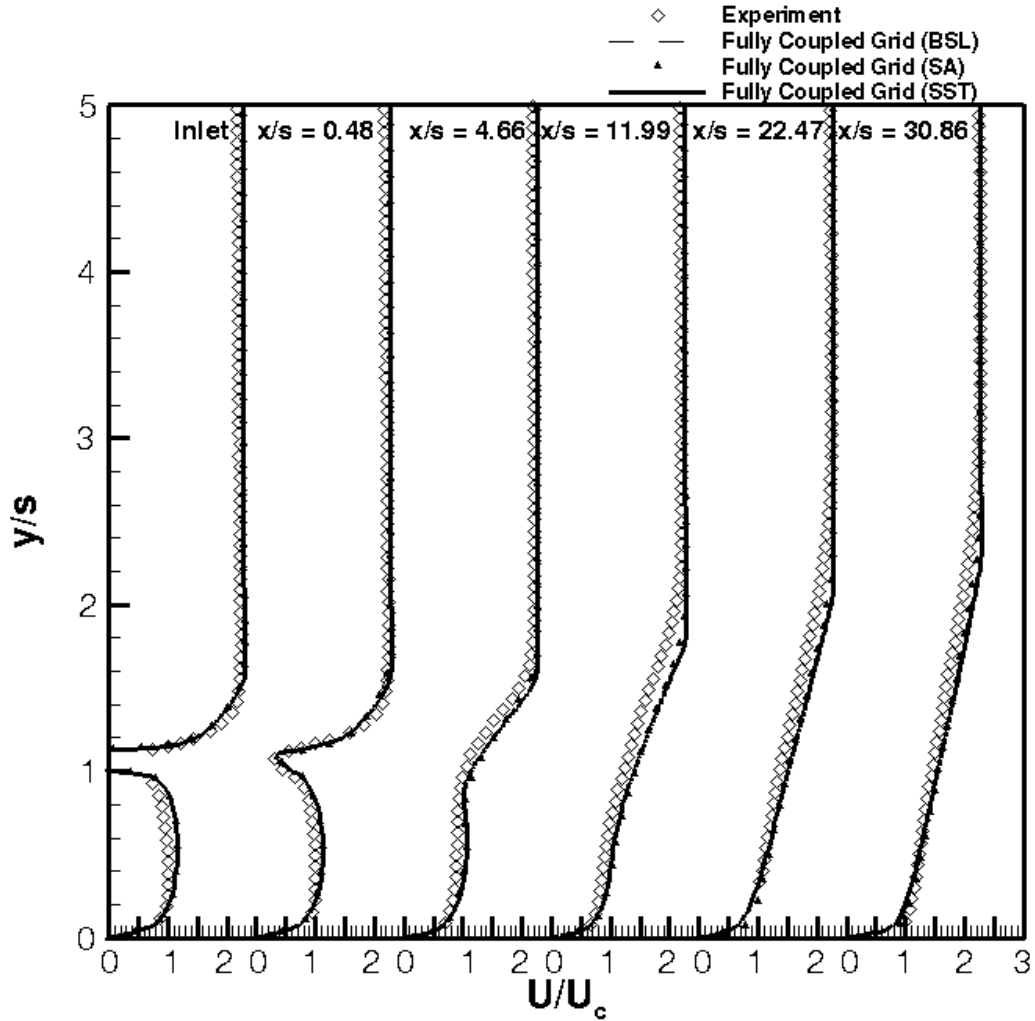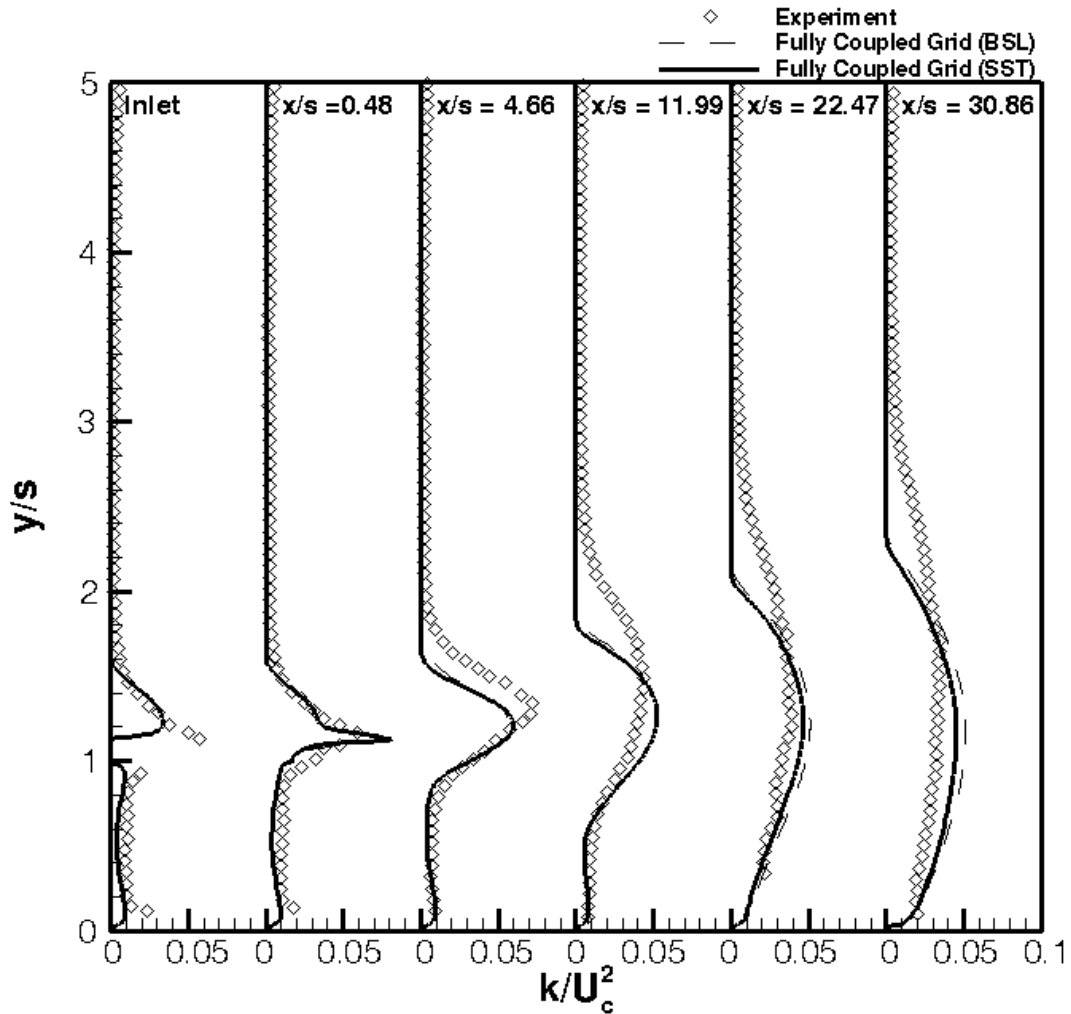
Figure 32. Comparison of velocity contours for the wall wake film cooling case.

mainstream momentum tends to diffuse into the coolant region causing the coolant

fluid to be accelerated due to the wall wake shear. By the final measurement stations,

the wall wake resembles a boundary layer and is very accurately characterized by the

simulation values. The BSL, SA and SST turbulence models captured the mean

experimental velocity within 15.0 %, 13.7% and 15.2 %, respectively.

Figure 33 shows the turbulent kinetic energy profile progression in the streamwise

direction for the wall wake experiment and the fully coupled RANS simulations

Figure 33. Comparison of turbulent kinetic energy contours for the wall wake film cooling case.

using all three turbulence models. The low initial level of turbulence in the inlet slot is captured to within 6.4 %, while the peak turbulent kinetic energy in the mainstream is within 14.8 % of the experimental values. As the streams progresses in the streamwise direction, the experimental turbulence spreads faster than the simulations, while the peak turbulent kinetic energy is reduced below the simulation value. This is distinctly different than the previous cases where the experimental turbulent kinetic energy always remains greater than the simulation values. The peak turbulent kinetic energy also moves to a lower wall normal position in the simulations than is predicted by

experiment, which shows that the location of the peak turbulence is not captured correctly. The sharp gradients at the extent of the mixing layer are once again present.

Figures 34 and 35 show temperature contours and flow effectiveness contours, respectively, for the wall wake experiment and RANS simulations at several different downstream stations. As is the case for all the previous RANS results, the thermal
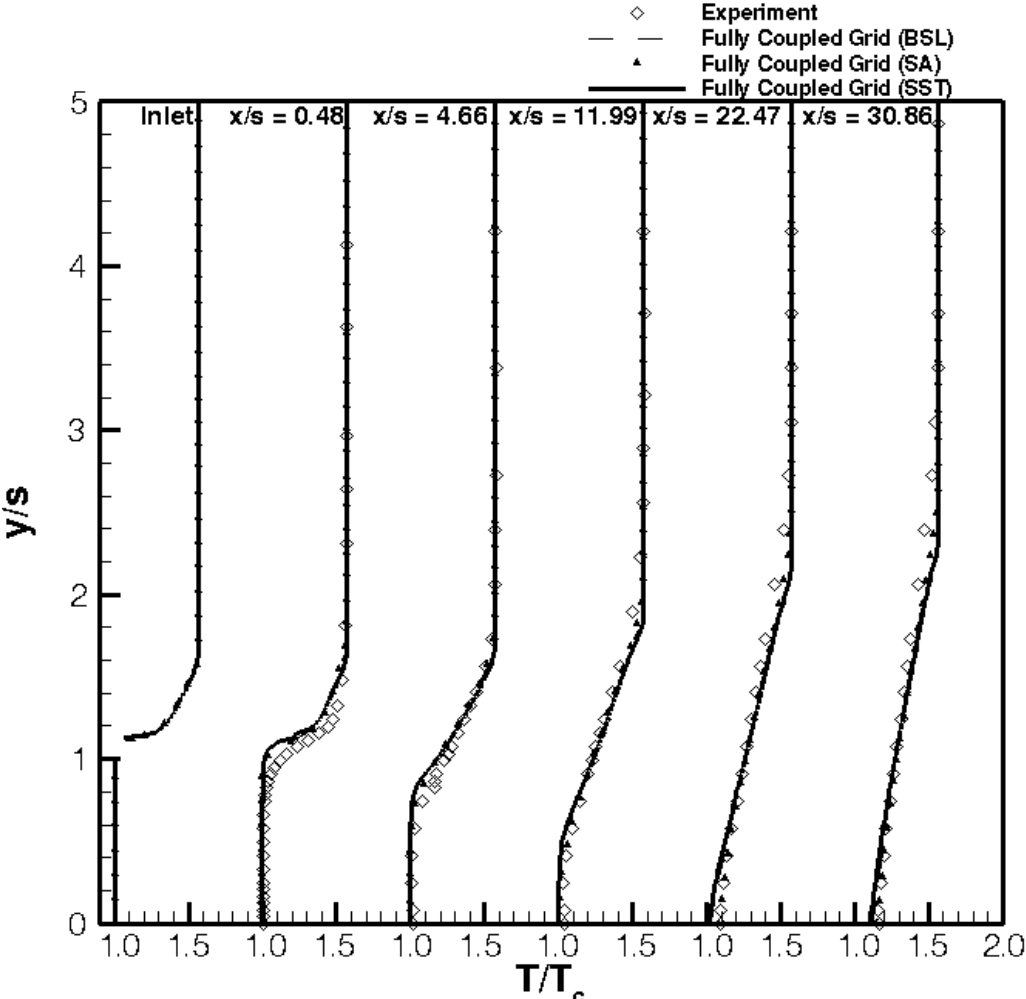
Figure 34. Comparison of temperature contours for the wall wake film cooling case.

mixing lags behind the experimental values, especially in the near wall region, resulting in higher effectivenesses as is seen in Figures 34 and 35. The spread rate is once again underpredicted and thermally these sharp gradients still exist in the flow. Relatively speaking, the thermal computational fields of the simulation best match the

experiment for this wall wake case, especially in terms of thermal mixing layer spread

rate. In fact the BSL, SA and SST capturing the temperature in the far field to within

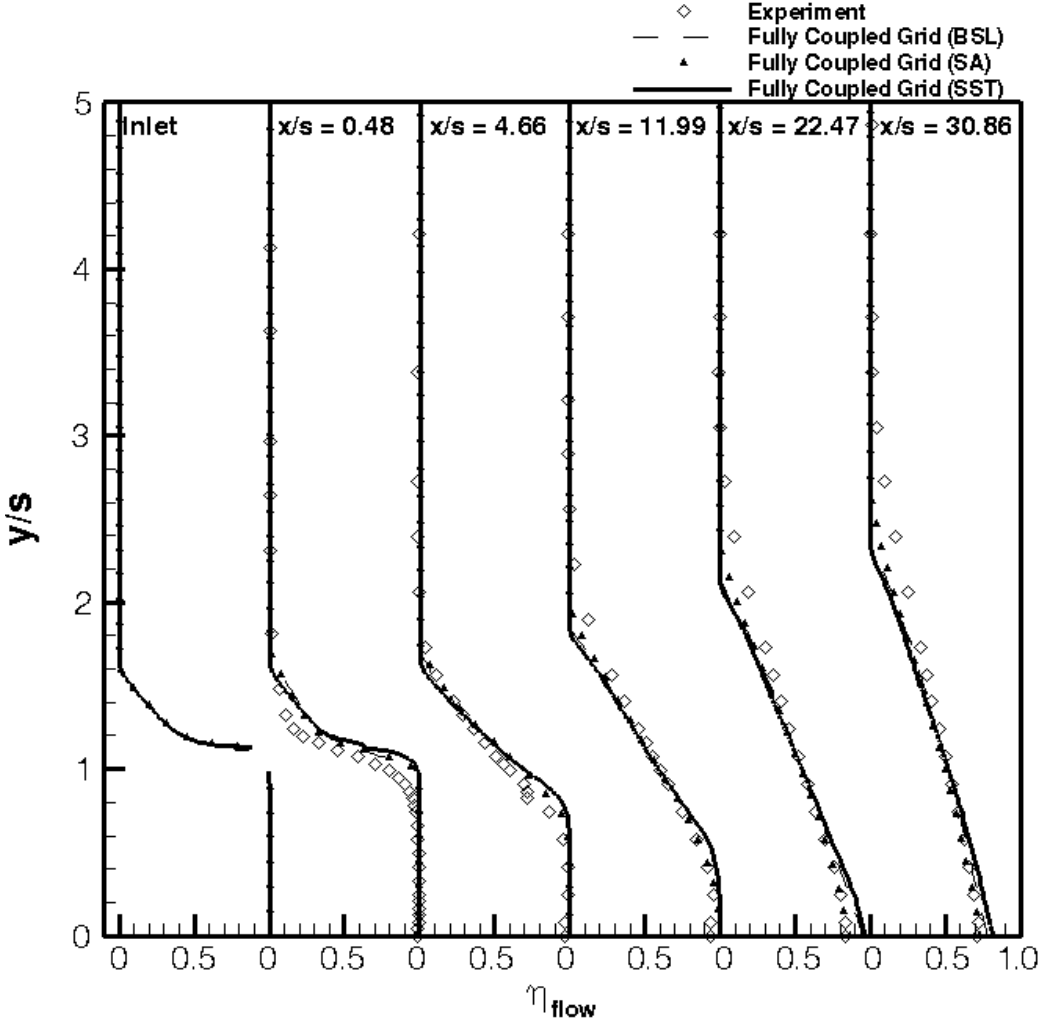5.9 %, 3.5 % and 5.9 %, respectively.

Figure 35. Comparison of flow effectiveness contours for the wall wake film cooling case.

Chapter 4: Conclusions

This study has presented a numerical investigation of subsonic adiabatic, turbulent slot film cooling. Three shear scenarios governing the film performance were considered (wall jet, wall wake and minimum shear), with the majority of the effort focused on the wall jet flow. For the wall jet, three mainstream precursor techniques were used in a RANS framework to explore the effects of turbulent inlet specification, inlet location, turbulence model and ensemble averaging. To better understand the mixing dynamics, an LES simulation was also performed. This LES simulation provided insights into the different mixing mechanisms relative to RANS models that allowed for more physical mixing. Namely, the large, coherent structures are responsible for the decay in the near injection field, which the RANS is incapable of resolving. For thoroughness, a turbulence model RANS case study was performed on both the minimum shear and wall wake cases.

4.1 Summary of Results

- Results show that computationally inexpensive RANS simulations *can* be used to obtain reasonable predictions of subsonic film cooling performance within 13%, 11% and 4.8% for the SST, BSL and SA turbulence models , depending on the strength and orientation of the shear.

- Mixing layer impingement on the wall is the reason for the curvature change in the streamwise progression of the wall effectiveness profile.

- Inlet plane needs to be moved upstream of the injection plane to avoid unphysical errors in the near-injection field.

- Differences between the mainstream precursor approaches are minor, as long as the inlet plane is moved upstream of the injection plane.

- The LES incompressible model provided the most accurate and physical film decay among the various simulations conducted in this thesis. Resolving large coherent structures allowed the LES to accurately predict the length of the potential core as well as the film decay trends over a large portion of the domain. The film decay rate in the far field is overpredicted with the constant density assumption. Figure 20 shows the underpredicted constant density LES velocity, which should lead to overprediction of the film decay rate as shown in Eq. 14.

- In this canonical configuration, all of the RANS models incorporate isotropic turbulence assumptions. All of the models considered overpredict the length of the ideal effectiveness region, due to the lack of bulk fluid transport into coolant stream and the underprediction of turbulent film mixing. The Spalart-Allmaras model performed the best of the turbulence models considered for all the film cooling cases. All the RANS models seemed to have delayed mixing, in which the far field mixing is accurately captured but the start of this far field mixing is delayed.

- The turbulence models produced similar trends in the adiabatic effectiveness curves, with the Spalart-Allmaras model performing the best of the models considered, while the SST, and BSL models perform nominally the same. All RANS study underpredict the mixing, which is in contrast to previous literature that states in certain instances namely in plane jet flows, these models overpredict the mixing.

- For the thin louver film cooling scenarios considered in this thesis, URANS was unable to reproduce large scale flow structures present in the flow. The URANS

simulations were found to provide nearly the same results as steady state RANS results and were therefore not shown.

• For this canonical configuration, the turbulence levels, in general, were underpredicted by the RANS models leading to lower mixing levels and therefore slower turbulent decay. The LES can resolve near injector mixing from bulk fluid transport via coherent structures, an example of which was shown in Figure 16. This turbulent mechanism is not found in RANS models because they view turbulence solely as enhanced diffusion instead of the subtly different bulk fluid transport leading to enhanced diffusion.

• Three mainstream precursor techniques were developed as part of this study. Since the mainstream precursor simulations provided similar film cooling results, the RANS film cooling simulation was shown to be relatively insensitive to the mainstream turbulence levels considered in this study. In light of this, the method requiring the least amount of inlet data, which is often unavailable, was used in the remainder of the study. The wind tunnel simulation requires no special, artificial processing in order for it to be used as a precursor simulation and requires only a mass flux, bulk temperature and temperature boundary conditions.

• The turbulence at the slot is crucial to near injector mixing physics. For the wall jet case, the LES best matched the experiment in terms of mean and turbulent kinematics, leading to more physical near injector mixing.

• Additionally, the effect of inlet location was also explored. The inlet must be moved upstream of the injection plane in order to avoid artificial acceleration or deceleration near the film cooling injection plane.

- The kinematics in the three film cooling scenarios were well predicted by all the RANS models. While the mixing layer spread rate and the gradients at the edge of the mixing layer were not accurately predicted, on the whole the kinematics matched the experimental data well. The thermal field showed larger deviations between the models depending on the near field or the far field mixing, suggesting that a constant turbulent Prandtl number is not always accurate.

4.2 Summary of Contributions

- Provided comparison of corrected comprehensive data set to both highly detailed RANS and LES data.

- Used mixing layer visualization to confirm the findings of Simon that mixing layer impingement causes the rapid decay in effectiveness and the end of the potential core.

- Bulk fluid transport from turbulent structures near the inlet cause the effectiveness to decay in the potential core, showing the RANS long potential core is not physical.

- RANS in general underpredicts the mixing, especially in the near injector field

- SA provides seemingly the best prediction of the film decay, but the performance models do not perform as the literature would suggest.

- Developed and documented several inlet techniques and explored their effect on film cooling performance.

- In this canonical configuration, the LES simulation showed the best performance, with the most physical film decay characteristics.

4.3 Suggestions for future work

•   Numerically simulate the hole injection in the coolant flow to understand how this injection changes the near injector behavior in RANS film cooling simulations.

•   To better and more fully compare the numerical mixing, a variable density LES calculation should be performed for all velocity ratios.

•   While RANS may not perform as well in the near injector region, perhaps a hybrid RANS-LES scheme would resolve bulk fluid transport from the mainstream to the wall.

•   Additionally wall models used in conjunction with coarse grid LES could be explored to see if the computational restrictions of LES calculations could be alleviated while not sacrificing accuracy.

Bibliography

[1]Sutton , G.P., "Rocket Propulsion Elements," John Wiley and Sons, New York, 5th edition, 198

[2]Lefebvre, A. H., *Gas Turbine Combustion*, Taylor & Francis, 1983

[3]Raffan, F., Experimental Characterization of Slot Film Cooling Flows With Minimally Intrusive Diagnostics, MS Thesis, University of Maryland at College Park, December 2008.

[4]Simon, F. F., "Jet Model for Slot Film Cooling With Effect of Free-Stream and Coolant Turbulence", NASA TP 2655, October 1986.

[5]Goldstein, R. J., Film Cooling, *in Advances in Heat Transfer*, vol. 7, Academic Press, New York, 1971. Pp. 321-378.

[6]Dellimore, K. Modeling and Simulation of Mixing Layer Flows for Rocket Engine Film Cooling, PhD Dissertation, University of Maryland at College Park, May 2010.

[7]Wilcox, D. C., "Turbulence Modeling: An Overview" in *Proceedings of the 39th Aerospace Sciences Meeting & Exhibit*, Reno, NV, January 8-11, 2001. AIAA Paper No. 2001-0724.

[8]Pajayakrit, P., and Kind, R. J, "Assessment and Modification of Two-EquationTurbulence Models", *AIAA Journal*, Vol. 38, No. 6, June 2000, pp. 955-963.

[9]Stoll, J. and Staub, J., "Film Cooling and Heat Transfer in Nozzles", *Journal of Turbomachinery*, Vol. 110, 1988, pp. 57-64.

[10]Zhou, J. M., Salcudean, M. and Gartshore, I. S. "A Numerical Computation of Film Cooling Effectiveness", *Near-Wall Turbulent Flows*, Elsevier Science Publishers, 1993, pp. 377-386.

[11]Jansson, L. S., Davidson, L. and Olsson, E., "Calculation of Steady and Unsteady Flows in a Film-Cooling Arrangement Using a Two-Layer Algebraic Stress Model", *Numerical Heat Transfer*, Part A., vol. 25, 1994, pp. 237-258.

[12]Lakehal, D., "Near-Wall Modeling of Turbulent Convective Heat Transport in Film Cooling of Turbine Blades with the Aid of Direct Numerical Simulation Data", *ASME Journal of Turbomachinery*, Vol. 124, 2002. pp. 485-498.

[13]Sinha, A. K., Bogard, D. G., and Crawford, M. E., "Film Cooling Effectiveness Downstream of a Single Row of Holes with Variable Density Ratio" *ASME Journal of Turbomachinery*. Vol. 113. 1991. pp. 442-449.

[14]Zhang, H., Tao, W., He, Y. and Zhang, W., "Numerical Study of Liquid Film Cooling in a Rocket Combustion Chamber", *International Journal of Heat and Mass Transfer*, Vol. 49, 2006, pp. 349-358.

[15]Cruz, C., Experimental and Numerical Characterization of Turbulent Slot Film Cooling, PhD Dissertation, University of Maryland at College Park, May 2008.

[16]Cruz, C., Marshall, A. "Surface and Gas Phase Temperature Near a Film Cooled Wall", AIAA-2004-3654, 2004.

[17]Dellimore, K., Marshall, A. Trouvé, A. and Cadou, C. "Numerical Simulation of Subsonic Slot-Jet Film Cooling of an Adiabatic Wall" *Proceedings of 47th AIAA Aerospace Sciences Meeting Including The New Horizons Forum and Aerospace Exposition*, January 5-8, 2009, Orlando, Fl. AIAA 2009-1577.

[18] Dellimore, K. Presentation entitled "Numerical Simulation of Subsonic Slot-Jet Film Cooling of an Adiabatic Wall", *47th AIAA Aerospace Sciences Meeting*. January 5-8, 2009, Orlando, Fl. AIAA 2009-1577.

[19] Matesanz, A., Velazquez, A., and Rodgriguez, M., "Numerical Simulation of Slot Film Cooling in Convergent-Divergent Nozzles", presented at the *29th AIAA/SAE/ASME/ASEE Joint Propulsion Conference and Exhibit*, Monterey, CA, AIAA paper 93-1977, 1993.

[20] Tyagi, M. and Acharya, S., "Large Eddy Simulation of Film Cooling Flow from an Incline Cylindrical Jet" *ASME Journal of Turbomachinery*, Vol. 125, 2003, pp. 734-742.

[21] Muldoon, F. and Acharya, S., "Analysis of k-ε Budgets for Film Cooling Using Direct Numerical Simulation" *AIAA Journal*, Vol. 44, No. 12, Dec. 2006. pp. 3010-3021.

[22] Lund, T. S., Wu, X., and Squires, K. D., "Generation of inflow data for the spatially-developing boundary layer simulations", *Journal of Computational Physics*, Vol. 140, Issue 2, pp. 233-258, 1998.

[23] E. A. Luke and X-L. Tong and J. Wu and P. Cinella, *CHEM 3.2: A Finite-Rate Viscous Chemistry Solver-The User Guide,* MSSU-COE-ERC-04-07 Mississippi State University, September, 2004.

[24] Luke, E. A. A Rule-Based Specification System for Computational Fluid Dynamics, PhD Dissertation, Mississippi State University, Starkville, MS, 1999.

[25] Tong, X-L., Luke, E. A., and Tang, L., "Evaluation of the Shear-Stress Transport Turbulence Model for Heat Transfer Applications," AIAA Paper 2003-0769, January 2003.

[26] Luke, E. A., Tong, X-L., Wu, J., Tang, L. and Cinnella, P., "A Step Towards 'Shape-Shifting' Algorithms: Reacting Flow Simulations Using Generalized Grids," AIAA Paper 2001-0897, January 2001.

[27] Pope, S. B., Turbulent Flows, Cambridge University Press, Cambridge, 2003.

[28] Spalart, P.R. and Allmaras, S. R., "A One-equation Turbulence Model for Aerodynamic Flows", AIAA-92-0439, 1992.

[29] Menter, F. R., "Two-Equation Eddy-Viscosity Turbulence Models for Engineering Applications" *AIAA Journal*, Vol. 32, No. 8, August 1994, pp. 1598-1605.

[30] Veluri, S. Roy, C. Hebert, S. and Luke, E. "Verification of the Loci-CHEM CFD Code using the Method of Manufactured Solutions" AIAA Paper 2008-661, January 2008.

[31] Veluri, S. Roy, C. and Choudhary, A. "Finite Volume Diffusion Operators for Compressible CFD on Unstructured Grids" AIAA Paper 2009-414, June 2009.

[32] Kays W.M., Crawford Michael E., Weigand Bernhard, "Convective Heat And Mass Transfer," 4th Ed., McGraw-Hill Education, United Kingdom, 2004

[33] Keating, A., Large-eddy simulation of heat transfer in the turbulent channel flow and in the turbulent flow downstream of a backward-facing step. PhD Thesis, Department of Mechanical Engineering, The University of Queensland, Brisbane, Australia, 2004.

[34] Piomelli, U., "Applications of Large Eddy Simulations in Engineering: An Overview". *Large Eddy Simulations of Complex Engineering and Geophysical Flows*. Cambridge University Press. 1993. Chap. 6. pp. 119-137.

[35] Chapman, D. R. "Computational aerodynamics development and outlook". *AIAA Journal*. 1979. Vol. 17. pp. 1293- 1313.